

Color Deconfinement and Charmonium Production in Nuclear Collisions

Louis Kluberg¹ and Helmut Satz²

¹ LLR, Ecole Polytechnique, CNRS-IN2P3, Palaiseau, France

² Fakultät für Physik, Universität Bielefeld, Bielefeld, Germany

Abstract:

In statistical QCD, color deconfinement and the properties of the quark-gluon plasma determine the in-medium behavior of heavy quark bound states. In high energy nuclear collisions, charmonia probe the partonic medium produced in the early stages of the interaction. We survey the present theoretical status and provide a critical evaluation of the charmonium production measurements in experiments at the CERN-SPS and the BNL-RHIC.

Contents

Introduction

I. Theory

1. Heavy Quarks and Quarkonia
2. Quarkonium Binding and Dissociation
3. Thermal Quark Dissociation
 - 3.1 Interaction Range and Color Screening
 - 3.2 Potential Models
 - 3.3 Lattice Studies of Charmonium Correlators
4. Charmonium Production in Hadronic Collisions
 - 4.1 Elementary Collisions
 - 4.2 p-A Collisions
 - 4.3 Nuclear Collisions
 - 4.4 Transverse Momentum Behavior
5. Conclusions

II. Experiment

1. Charmonium Experiments at the CERN SPS
 - 1.1 The Nuclear Dependence of Charmonium Production
 - 1.2 Normal Charmonium Production
 - 1.3 The First Hints of an Anomaly in Pb-Pb Collisions
 - 1.4 Anomalous J/ψ suppression in Pb-Pb Collisions
2. Features of ψ' Suppression at SPS energies
3. More Results from SPS and RHIC
 - 3.1 J/ψ Suppression in In-In Collisions at 158 GeV
 - 3.2 J/ψ Suppression in A-A Collisions at $\sqrt{s} = 200$ GeV

4. Discussion and Evaluation

5. Summary of the Experimental Status

Outlook

References

Introduction

Statistical QCD predicts that strongly interacting matter undergoes a deconfining transition to a new state, the quark-gluon plasma, in which the colored quarks and gluons are no longer bound to colorless hadrons. How can this state be investigated - which phenomena provide information about its thermal properties? The main probes considered so far are electromagnetic signals (real or virtual photons), heavy flavor mesons ($Q\bar{q}/\bar{Q}q$ states), quarkonia ($Q\bar{Q}$ pairs), and jets (energetic partons). In theory, the ultimate aim is to carry out *ab initio* calculations of the in-medium behavior of these probes in finite temperature QCD. In high energy nuclear collisions, we want to study the deconfinement transition and the QGP in the laboratory, to compare experimental results to QCD predictions. In our report, we want to consider as specific case the spectral analysis of quarkonia in a hot QGP and its application to nuclear collisions.

The theoretical basis for this analysis is:

- The QGP consists of deconfined color charges, so that the binding of a $Q\bar{Q}$ pair in such a medium is subject to the effects of color screening.
- The color screening radius $r_D(T)$ decreases with temperature T .
- When $r_D(T)$ falls below the binding radius r_i of a $Q\bar{Q}$ state i , the Q and the \bar{Q} can no longer bind, so that quarkonium i cannot exist.
- The quarkonium dissociation points T_i , specified through $r_D(T_i) \simeq r_i$, determine energy density and temperature of the QGP, as schematically illustrated in Fig. 1.

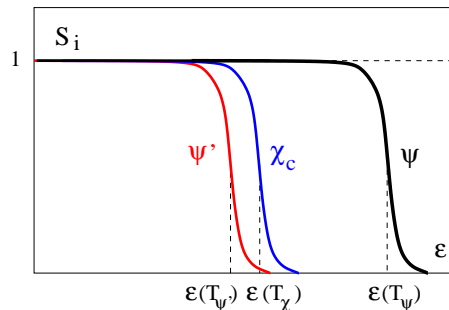


Figure 1: Charmonium survival probabilities vs. energy density

Clearly the essential aspect here is a precise determination of the dissociation points of the different quarkonium states, in temperature and/or energy density. This will therefore be the primary task of theoretical studies of the in-medium behavior of quarkonia.

Quarkonium production in high energy collisions provides an excellent experimental tool to address a variety of challenging questions.

- In pA collisions, quarkonium production can be studied in cold nuclear matter, in order to provide a reference to determine which features of AA collisions are “anomalous”, i.e., due to a newly produced medium.
- In AA collisions, quarkonium production can be measured as function of collision energy, centrality, transverse momentum, and A , providing a variety of different conditions of the produced medium.

- The onset of anomalous suppression for the different quarkonium states can be determined and correlated to thermodynamic variables, such as the temperature or the energy density.
- The resulting thresholds in the survival probabilities S_i of states i can then be compared to the relevant QCD predictions of Fig. 1.

In this way we could, at least in principle, obtain a direct comparison between experimental results and quantitative predictions from finite temperature QCD.

Starting its operation at CERN in 1986, immediately after the theoretical prediction [1] of J/ψ suppression as deconfinement signal, the experiment NA38 pioneered the systematic study of J/ψ production and suppression. It was followed, some years later, by experiments NA50 and NA51, with adapted and upgraded versions of the same detector. The first of these experiments, NA38, had submitted a Letter of Intent in 1984 aiming at the study of thermal muon pair production. It was on the floor in 1986, but it had changed its main physics goal, as stated in its original proposal, to the study of J/ψ suppression. The three experiments made use of an exceptionally performant muon pair spectrometer with good measurement resolution and high luminosity operating capability; both features were inherited from the previous NA10 experiment, which was designed for and devoted to the study of high mass Drell-Yan muon pairs. It took almost 20 years of efforts to improve the detectors and beams, refine the analyses, overcome various difficulties and collect useful data under various experimental conditions. This allowed double, and sometimes triple checks of the outcoming results. In the meantime, new results are presently being provided by much more recent experiments, PHENIX at the BNL-RHIC collider and NA60 at the CERN-SPS.

The main issue to be addressed is whether an *anomalous* J/ψ suppression has or has not been discovered, as claimed in past publications. In order to answer this question, independently from any theoretical model, a mandatory prerequisite is to unambiguously define and precisely establish what is or should be considered *normal* J/ψ behavior. We will see that the investment required to fill this part of the paradigm is always huge and, moreover, specific to each set of experimental conditions. It is, nevertheless, a *sine qua non* condition to avoid an insurmountable potential dead end to the problem.

I Theory

1 Heavy Quarks and Quarkonia

Heavy quarks first showed up in the discovery of the J/ψ meson [2], of mass of 3.1 GeV; it is a bound state of a charm quark (c) and its antiquark (\bar{c}), each having a mass of some 1.2–1.5 GeV. On the next level there is the Υ meson [3], with a mass of about 9.5 GeV, made up of a bottom or quark-antiquark pair ($b\bar{b}$), with each quark here having a mass around 4.5 - 4.8 GeV. Both charm and bottom quarks can of course also bind with normal light quarks, giving rise to open charm (D) and open beauty (B) mesons. The lightest of these ‘light-heavy’ mesons have masses of about 1.9 GeV and 5.3 GeV, respectively.

The bound states of a heavy quark Q and its antiquark \bar{Q} are generally referred to as quarkonia. Besides the initially discovered vector ground states J/ψ and Υ , both the $c\bar{c}$ and the $b\bar{b}$ systems give rise to a number of other *stable* bound states of different quantum numbers. They are stable in the sense that their mass is less than that of two light-heavy mesons, so that strong decays into open charm or beauty are forbidden. The measured stable charmonium spectrum contains the $1S$ scalar η_c and vector J/ψ , three $1P$ states χ_c (scalar, vector and tensor), and the $2S$ vector state ψ' , whose mass is just below the open charm threshold. There are further charmonium states above the ψ' ; these can decay into $D\bar{D}$ pairs, and we shall here restrict our considerations only to quarkonia stable under strong interactions. These are summarized in tables 1 and 2 for charmonia and bottomonia, respectively. The binding energies ΔE listed there are the differences between the quarkonium masses and the open charm or beauty threshold, respectively.

state	η_c	J/ψ	χ_{c0}	χ_{c1}	χ_{c2}	ψ'
mass [GeV]	2.98	3.10	3.42	3.51	3.56	3.69
ΔE [GeV]	0.75	0.64	0.32	0.22	0.18	0.05

Table 1: Charmonium states and binding energies

state	Υ	χ_{b0}	χ_{b1}	χ_{b2}	Υ'	χ'_{b0}	χ'_{b1}	χ'_{b2}	Υ''
mass [GeV]	9.46	9.86	9.89	9.91	10.02	10.23	10.26	10.27	10.36
ΔE [GeV]	1.10	0.70	0.67	0.64	0.53	0.34	0.30	0.29	0.20

Table 2: Bottomonium states and binding energies

Quarkonia are rather unusual hadrons. The masses of the light hadrons, in particular those of the non-strange mesons and baryons, arise almost entirely from the interaction energy of their nearly massless quark constituents. In contrast, the quarkonium masses are largely determined by the bare charm and bottom quark masses. These large quark masses allow a very straightforward calculation of many basic quarkonium properties, using non-relativistic potential theory. It is found that the ground states and the lower excitation levels of quarkonia are very much smaller than the normal hadrons, and that they are very tightly bound. Now deconfinement is a matter of scales: when the separation between normal hadrons becomes much less than the size of these hadrons, they melt to form the quark-gluon plasma. What happens at this point to the much smaller quarkonia? When do they become dissociated? As already indicated, the disappearance of quarkonia can signal the presence of a deconfined medium [1], and the melting of specific quarkonium states can determine the temperature of this medium [4]. Thus the study of the quarkonium spectrum in a given medium is akin to the spectral analysis of stars [5], where the presence or absence of specific excitation or absorption lines allows a determination of the temperature of the stellar matter.

After these introductory comments, we shall review the basic properties of quarkonia and the dynamics of their dissociation, and then survey the different approaches to quarko-

nium binding in QCD thermodynamics. Following this, we consider the main theoretical features of quarkonium production in elementary as well as $p - A$ and nucleus-nucleus collisions. With the theoretical basis provided, we then address the present experimental results.

2 Quarkonium Binding and Dissociation

We had defined quarkonia as bound states of heavy quarks which are stable under strong decay into open heavy flavor, i.e., $M_{c\bar{c}} \leq 2M_D$ for charmonia and $M_{b\bar{b}} \leq 2M_B$ for bottomonia. Since the quarks are so heavy, quarkonium spectroscopy can be studied quite well in non-relativistic potential theory [7]. The simplest (“Cornell”) confining potential [8] for a $Q\bar{Q}$ at separation distance r has the form

$$V(r) = \sigma r - \frac{\alpha}{r} \quad (1)$$

with a string tension $\sigma \simeq 0.2 \text{ GeV}^2$ and a Coulomb-like term with a gauge coupling $\alpha \simeq \pi/12$. The corresponding Schrödinger equation

$$\left\{ 2m_c - \frac{1}{m_c} \nabla^2 + V(r) \right\} \Phi_i(r) = M_i \Phi_i(r) \quad (2)$$

then determines the bound state masses M_i and the wave functions $\Phi_i(r)$, and with

$$\langle r_i^2 \rangle = \int d^3r r^2 |\Phi_i(r)|^2 / \int d^3r |\Phi_i(r)|^2. \quad (3)$$

the latter in turn provide the (squared) average bound state diameters.

The solution of eq. (2) gives in fact a very good account of the full (spin-averaged) quarkonium spectroscopy, as seen in Table 3. The line labelled ΔM shows the differences between the experimental and the calculated values; they are in all cases less than 1 %. Here r_0 gives the $Q\bar{Q}$ separation for the state in question, and the input parameters are $m_c = 1.25 \text{ GeV}$, $m_b = 4.65 \text{ GeV}$, $\sqrt{\sigma} = 0.445 \text{ GeV}$, $\alpha = \pi/12$ [9].

state	J/ψ	χ_c	ψ'	Υ	χ_b	Υ'	χ'_b	Υ''
mass [GeV]	3.10	3.53	3.68	9.46	9.99	10.02	10.26	10.36
ΔE [GeV]	0.64	0.20	0.05	1.10	0.67	0.54	0.31	0.20
ΔM [GeV]	0.02	-0.03	0.03	0.06	-0.06	-0.06	-0.08	-0.07
r_0 [fm]	0.50	0.72	0.90	0.28	0.44	0.56	0.68	0.78

Table 3: Quarkonium Spectroscopy from Non-Relativistic Potential Theory [9]

We thus see that in particular the J/ψ and the lower-lying bottomonium states are very tightly bound ($2M_{D,B} - M_0 \gg \Lambda_{\text{QCD}}$) and of very small spatial size ($r_0 \ll r_h \simeq 1.5 - 2 \text{ fm}$); here r_h denotes the typical hadron diameter. Through what kind of interaction dynamics can they then be dissociated?

As illustration, we consider the collision dissociation of a J/ψ . It is very small ($r_{J/\psi} \sim 0.5$ fm) and hence can only be resolved by a sufficiently hard probe [10]. It is moreover tightly bound ($2M_D - M_{J/\psi} \sim 0.6$ GeV), so that only a sufficiently energetic projectile can break the binding. In the collision with a normal hadron, the J/ψ can thus only be dissociated through the interaction with a hard gluonic constituent of the hadron, not with the hadron as a whole (see Fig. 2).

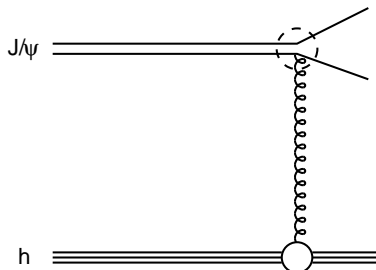


Figure 2: J/ψ -hadron interaction

The gluon momentum distribution $g(x)$ in a hadron is determined in deep inelastic lepton-hadron scattering; with k_h denoting the gluon momentum, $x = k_h/p_h$ specifies the fraction of the incident hadron momentum p_h carried by the gluon. For mesons, one finds for large momenta

$$g(x) \sim (1-x)^3, \quad (4)$$

so that the average momentum of a hadronic gluon is

$$\langle k \rangle_h = \frac{1}{5} \langle p_h \rangle. \quad (5)$$

For thermal hadrons in confined matter, $\langle p_h \rangle \sim 3T$, with $T < 175$ MeV, so that with

$$\langle k \rangle_h = \frac{3}{5} T \leq 0.1 \text{ GeV} \ll \Delta E \simeq 0.6 \text{ GeV} \quad (6)$$

the gluon momentum is far too low to allow a dissociation of the J/ψ .

On the other hand, the average momentum of a deconfined thermal gluon in a quark-gluon plasma will be

$$\langle k_g \rangle \simeq 3 T \quad (7)$$

and for $T \gtrsim 1.2 T_c$, this provides enough energy to overcome the J/ψ binding. We thus expect that a hot deconfined medium can lead to J/ψ dissociation, while the gluons available in a confined medium are too soft to allow this.

To make these considerations quantitative, one first has to calculate the cross-section for the gluon-dissociation of a J/ψ , a QCD analogue of the photo-effect. This can be carried out using the operator product expansion [10, 11], and the result is

$$\sigma_{g-J/\psi} \sim \frac{1}{m_c^2} \frac{(k/\Delta E_\psi - 1)^{3/2}}{(k/\Delta E_\psi)^5} \quad (8)$$

with $\Delta E_{J/\psi} = 2M_D - M_{J/\psi}$. The corresponding cross-section for the hadron dissociation is then obtained by convoluting the gluon-dissociation cross-section (8) with the hadronic gluon distribution function $g(x)$, which for J/ψ -meson interactions leads to

$$\sigma_{h-J/\psi} \simeq \sigma_{\text{geom}}(1 - \lambda_0/\lambda)^{5.5} \quad (9)$$

with $\lambda \simeq (s - M_\psi^2)/M_\psi$ and $\lambda_0 \simeq (M_h + \Delta E_\psi)$. Here $\sigma_{\text{geom}} \simeq \pi(r_{J/\psi}/2)^2 \simeq 2$ mb is the geometric J/ψ cross-section and M_h denotes the mass of the incident meson. In Fig. 3, we compare the two dissociation cross-sections (8) and (9) as function of the incident projectile momentum.

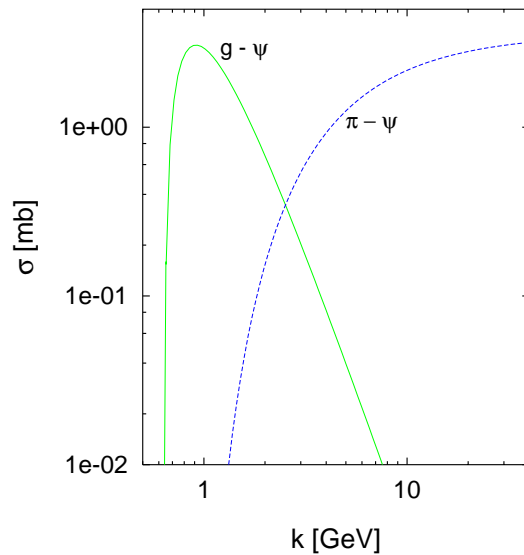


Figure 3: Gluon and hadron J/ψ dissociation cross-sections [10]

This result confirms the qualitative arguments given at the beginning of this section: typical thermal gluon momenta near 1 GeV produce a large dissociation cross-section, whereas hadron momenta in a thermal range (up to 2 - 3 GeV) still lead to a vanishingly small cross-section. In other words, the J/ψ should survive in confining media, but become dissociated in a hot quark-gluon plasma [10].

The calculations leading to eq. (8) are exact in the large quark mass limit $m_Q \rightarrow \infty$. It is not clear if the charm quark mass really satisfies this condition, and so the dissociation cross section in J/ψ -hadron collisions has been discussed in other approaches, some of which lead to much larger values [12,13]. The basic question is apparently whether or not the charmonium wave function has enough overlap with that of the usual hadrons to lead to a sizeable effect. It may well be that this question is resolvable only experimentally, by testing if slow charmonia in normal nuclear matter suffer significant dissociation. Such experiments are definitely possible [14].

3 Thermal Quarkonium Dissociation

We shall here address the first of our “basic” questions: Is it possible to specify the state of strongly interacting matter in terms of observable quantities calculated in QCD?

3.1 Interaction Range and Color Screening

Consider a color-singlet bound state of a heavy quark Q and its antiquark \bar{Q} , put into the medium in such a way that we can measure the energy of the system as function of the $Q\bar{Q}$ separation r (see Fig. 4). The quarks are assumed to be heavy so that they are static and any energy changes indicate changes in the binding energy. We consider first the case of vanishing baryon density; at $T = 0$, the box is therefore empty.

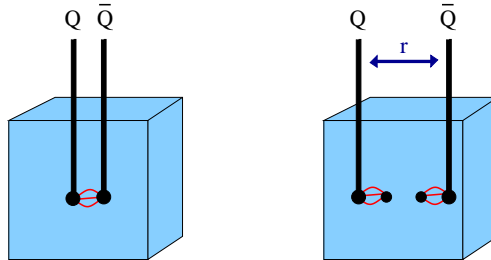


Figure 4: String breaking for a $Q\bar{Q}$ system

In vacuum, i.e., at $T = 0$, the free energy of the $Q\bar{Q}$ pair is assumed to have the string form [8]

$$F(r) \sim \sigma r \quad (10)$$

where $\sigma \simeq 0.16 \text{ GeV}^2$ is the string tension as determined in the spectroscopy of heavy quark resonances (charmonium and bottomonium states). Thus $F(r)$ increases with separation distance; but when it reaches the value of a pair of dressed light quarks (about the mass of a ρ meson), it becomes energetically favorable to produce a $q\bar{q}$ pair from the vacuum, break the string and form two light-heavy mesons ($Q\bar{q}$) and ($\bar{Q}q$). These can now be separated arbitrarily far without changing the energy of the system (Fig. 4).

The string breaking energy for charm quarks is found to be

$$F_0 = 2(M_D - m_c) \simeq 1.2 \text{ GeV}; \quad (11)$$

for bottom quarks, one obtains the same value,

$$F_0 = 2(M_B - m_b) \simeq 1.2 \text{ GeV}, \quad (12)$$

using in both cases the quark mass values obtained in the solution leading to Table 3. Hence the onset of string breaking is evidently a property of the vacuum as a medium. It occurs when the two heavy quarks are separated by a distance

$$r_0 \simeq 1.2 \text{ GeV}/\sigma \simeq 1.5 \text{ fm}, \quad (13)$$

independent of the mass of the (heavy) quarks connected by the string.

If we heat the system to get $T > 0$, the medium begins to contain light mesons, and the large distance $Q\bar{Q}$ free energy $F(\infty, T)$ decreases, since we can use these light hadrons to achieve an earlier string breaking through a kind of flip-flop recoupling of quark constituents [15], resulting in an effective screening of the interquark force (see Fig. 5). Near

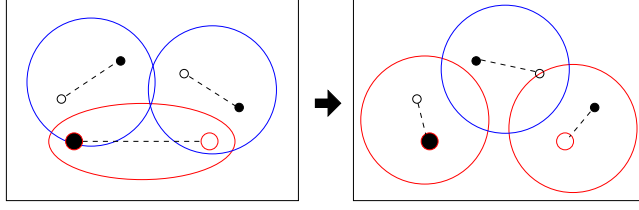


Figure 5: In-medium string breaking through recoupling

the deconfinement point, the hadron density increases rapidly, and hence the recoupling dissociation becomes much more effective, causing a considerable decrease of $F(\infty, T)$.

A further increase of T will eventually bring the medium to the deconfinement point T_c , at which chiral symmetry restoration causes a rather abrupt drop of the light quark dressing (equivalently, of the constituent quark mass), increasing strongly the density of constituents. As a consequence, $F(\infty, T)$ now continues to drop sharply. Above T_c , light quarks and gluons become deconfined color charges, and this quark-gluon plasma leads to a color screening, which limits the range of the strong interaction. The color screening radius r_D , which determines this range, is inversely proportional to the density of charges, so that it decreases with increasing temperature. As a result, the $Q\bar{Q}$ interaction becomes more and more short-ranged.

In summary, starting from $T = 0$, the $Q\bar{Q}$ probe first tests vacuum string breaking, then a screening-like dissociation through recoupling of constituent quarks, and finally genuine color screening. In Fig. 6, we show the behavior obtained in full two-flavor QCD for the color-singlet $Q\bar{Q}$ free energy as a function of r for different T [16].

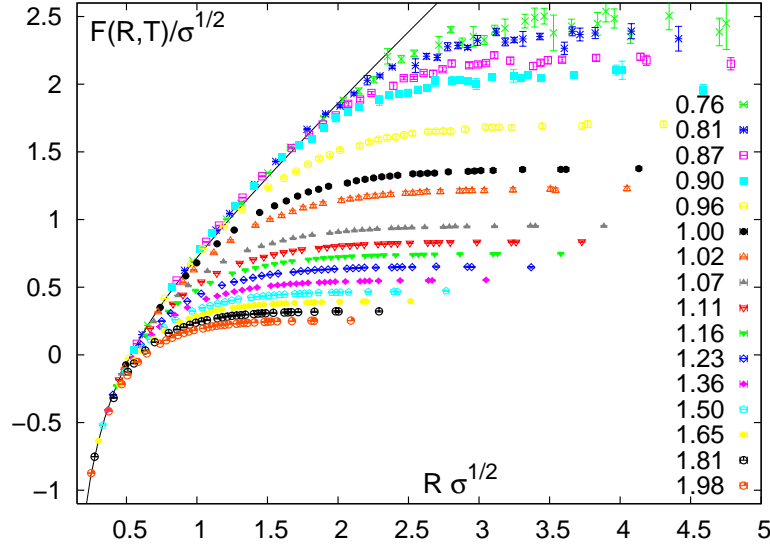


Figure 6: The color singlet $Q\bar{Q}$ free energy $F(r, T)$ vs. r at different T [16]

It is evident in Fig. 6 that the asymptotic value $F(\infty, T)$, i.e., the energy needed to separate the $Q\bar{Q}$ pair, decreases with increasing temperature, as does the separation distance at which “the string breaks”. Here we consider the latter to be defined by

the point beyond which the free energy remains constant within errors. The behavior of both quantities is shown in Fig. 7. Deconfinement is thus reflected very clearly in the temperature behavior of the free energy of a heavy quark potential: both the string breaking energy and the interaction range drop sharply around T_c . The latter decreases from hadronic size in the confinement region to much smaller values in the deconfined medium, where color screening is operative.

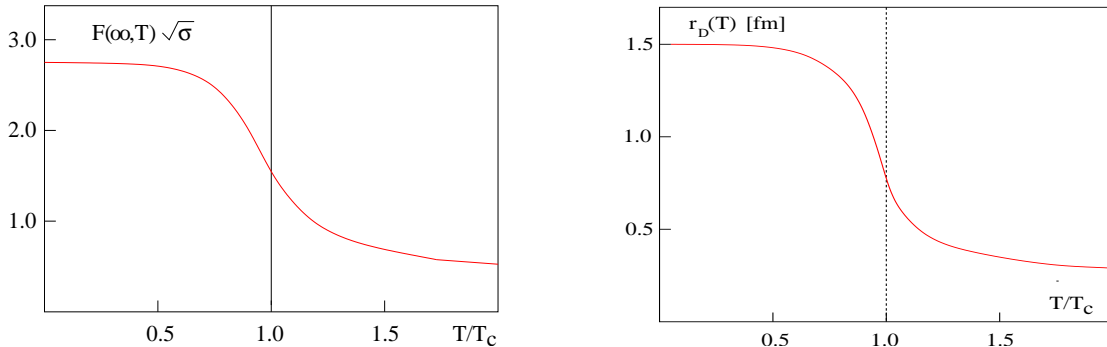


Figure 7: Asymptotic free energy and interaction range at different temperatures

The in-medium behavior of heavy quark bound states thus serves quite well as probe of the state of matter in QCD thermodynamics. We had so far just considered $Q\bar{Q}$ bound states in general. Let us now turn to a specific state such as the J/ψ . What happens when the range of the binding force becomes smaller than the radius of the state? Since the c and the \bar{c} can now no longer see each other, the J/ψ must dissociate for temperatures above this point. Hence the dissociation points of the different quarkonium states provide a way to measure the temperature of the medium. The effect had already been illustrated schematically in Fig. 1, showing how with increasing temperature the different charmonium states disappear sequentially as function of their binding strength; the most loosely bound state disappears first, the ground state last.

Moreover, since finite temperature lattice QCD also provides the temperature dependence of the energy density, the melting of the different charmonia or bottomonia can be specified as well in terms of ϵ . In Fig 8, we illustrate this, combining the the energy density calculated in lattice QCD [18, 19] and the force radii from Fig. 7. It is evident that although ψ' and χ_c are expected to melt around T_c , the corresponding dissociation energy densities will presumably be quite different.

To make these considerations quantitative, we thus have to find a way to determine the in-medium melting points of the different quarkonium states. This problem has been addressed in two different approaches:

- Solve the Schrödinger equation (2) with a temperature-dependent potential $V(r, T)$, obtained either through model considerations or from heavy quark lattice studies.
- Calculate the quarkonium spectrum directly in finite temperature lattice QCD.

Clearly the last is the only model-independent way, and it will in the long run provide the decisive determination. However, the direct lattice study of charmonium spectra has become possible only quite recently, and corresponding studies for bottomonia are

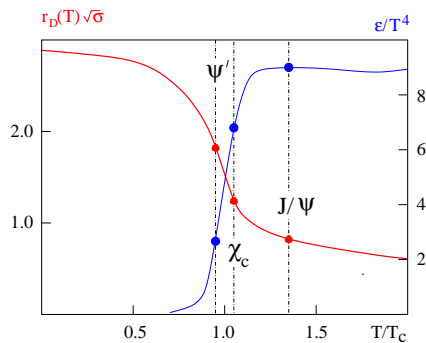


Figure 8: Charmonium dissociation vs. temperature and energy density

still more difficult. Hence much of what is known so far is based on Schrödinger equation studies with different model inputs. To illustrate the model-dependence of the dissociation parameters, we first cite early work modelling the temperature dependence of $V(r, T)$, then some more recent studies based on lattice results for $F(r, T)$, and finally summarize the present state of direct lattice calculations of charmonia in finite temperature media.

3.2 Potential Model Studies

The first quantitative studies of finite temperature charmonium dissociation [4, 5] were based on screening in the form obtained in one-dimensional QED, the so-called Schwinger model. The confining part of the Cornell potential (1), $V(r) \sim \sigma r$, is the solution of the Laplace equation in one space dimension. In this case, Debye-screening leads to [21]

$$V(r, T) \sim \sigma r \left\{ \frac{1 - e^{-\mu r}}{\mu r} \right\}, \quad (14)$$

where $\mu(T)$ denotes the screening mass (inverse Debye radius) for the medium at temperature T . This form reproduces at least qualitatively the convergence to a finite large distance value $V(\infty, T) = \sigma/\mu(T)$, and since $\mu(T)$ increases with T , it also gives the expected decrease of the potential with increasing temperature. Combining this with the usual Debye screening for the $1/r$ part of eq. (1) then leads to

$$V(r, T) \sim \sigma r \left\{ \frac{1 - e^{-\mu r}}{\mu r} \right\} - \frac{\alpha}{r} e^{-\mu r} = \frac{\sigma}{\mu} \left\{ 1 - e^{-\mu r} \right\} - \frac{\alpha}{r} e^{-\mu r} \quad (15)$$

for the screened Cornell potential. In [4], the screening mass was assumed to have the form $\mu(T) \simeq 4 T$, as obtained in first lattice estimates of screening in high temperature $SU(N)$ gauge theory. Solving the Schrödinger equation with these inputs, one found that both the ψ' and the χ_c become dissociated essentially at $T \simeq T_c$, while the J/ψ persisted up to about $1.2 T_c$. Note that as function of the energy density $\epsilon \sim T^4$, this meant that the J/ψ really survives up to much higher ϵ .

This approach has two basic shortcomings:

- The Schwinger form (14) corresponds to the screening of σr in one space dimension; the correct result in three space dimensions is different [21].

- The screening mass $\mu(T)$ is assumed in its high energy form; lattice studies show today that its behavior near T_c is quite different [23].

While the overall behavior of this approach provides some first insight into the problem, quantitative aspects require a more careful treatment.

From thermodynamics it is known that F can be decomposed into the internal energy U and the entropy S of the system,

$$F = U - TS. \quad (16)$$

Since

$$F = -T \ln Z \quad (17)$$

in terms of the partition function Z , we have

$$U = -T^2 \left(\frac{\partial[F/T]}{\partial T} \right) \quad (18)$$

and

$$S = - \left(\frac{\partial F}{\partial T} \right). \quad (19)$$

Given $F(r, T)$, eqns. (18) and (19) determine $U(r, T)$ and $S(r, T)$. It should be emphasized that the $F(r, T)$ calculated in finite temperature lattice QCD specifies the difference in free energy between a system with and a system without a $Q\bar{Q}$ pair, so that also U and S are such differences. Since $U(r, T)$ thus is the expectation value of the the Hamiltonian with a heavy quark pair, minus that without such a pair, it is the relevant quantity to determine the binding potential. We shall see shortly, however, that other effects enter as well.

When the first lattice results for the color averaged value $F_{\text{av}}(r, T)$ of the free energy became available, they were used to determine melting points for the different charmonium states [22]. It was assumed that in the thermodynamic relation (18) the entropy term $-T(\partial F/\partial T)$ could be neglected, thus equating binding potential and free energy,

$$V(r, T) \simeq F_{\text{av}}(r, T). \quad (20)$$

Using this potential in the Schrödinger equation (2) specifies the temperature dependence of the different charmonium masses. On the other hand, the large distance limit of $V(r, T)$ determines the temperature variation of the open charm meson D ,

$$2M_D(T) \simeq 2m_c + V(\infty, T) \quad (21)$$

In fig. 9, we compare the resulting open and hidden charm masses as function of temperature. It is seen that the ψ' mass falls below $2 M_D$ around $0.2 T_c$, that of the χ_c at about $0.8 T_c$; hence these states disappear by strong decay at the quoted temperatures. Only the ground state J/ψ survives up to T_c and perhaps slightly above; the lattice data available at the time did not extend above T_c , so further predictions were not possible.

The main shortcoming of this approach is also quite evident. The neglect of the entropy term in the potential reduces $V(r, T)$ and hence the binding. As a result, the D mass drops faster with temperature than that of the charmonium states, and it is this effect

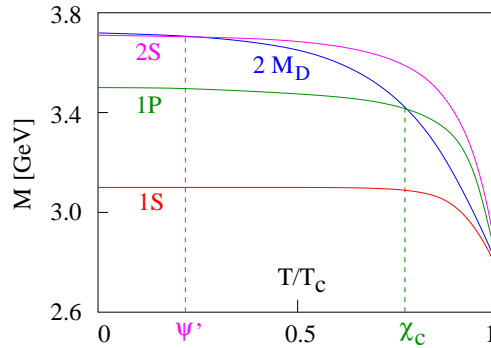


Figure 9: Temperature dependence of open and hidden charm masses [22]

which leads to the early charmonium dissociation. Moreover, in the lattice studies used here, only the color averaged free energy was calculated, which leads to a further reduction of the binding force.

Today, finite temperature lattice QCD with two light quark flavors [16, 17] provides the *color singlet* free energy $F(r, T)$ of a static $Q\bar{Q}$ pair in a strongly interacting medium at temperature T . Here $F(r, T)$ is again the difference between a system with and a system without a $Q\bar{Q}$ pair; it was shown in Fig. 6 for several temperatures below and above the deconfinement point T_c . For very small separation $r \ll T^{-1}$, the $Q\bar{Q}$ pair as a color neutral entity does not “see” the medium. Hence the results for different temperatures must coincide in the short distance limit and fall on the $T = 0$ curve $F(r, T = 0) = \sigma r - \alpha/r$; this is used to normalize the results for $T > T_c$. Given $F(r, T)$, we can now extract the corresponding color singlet behavior of the internal energy and the entropy; in Fig. 10, we show schematically the resulting behavior of the different thermodynamic potentials as function of r at some fixed $T > T_c$ and as function of T for $r \rightarrow \infty$ [24]. At very short $Q\bar{Q}$ separation distance and finite T , for $r \ll T^{-1}$, the $Q\bar{Q}$ feels no medium and the medium does not see the pair; hence $U(r, T) = F(r, T) = F(r, 0)$ and $S(r, T) = 0$. The onset of the entropy starts around $r \simeq r_D(T)$, i.e, when the $Q\bar{Q}$ separation distance reaches the value of the screening length of the medium.

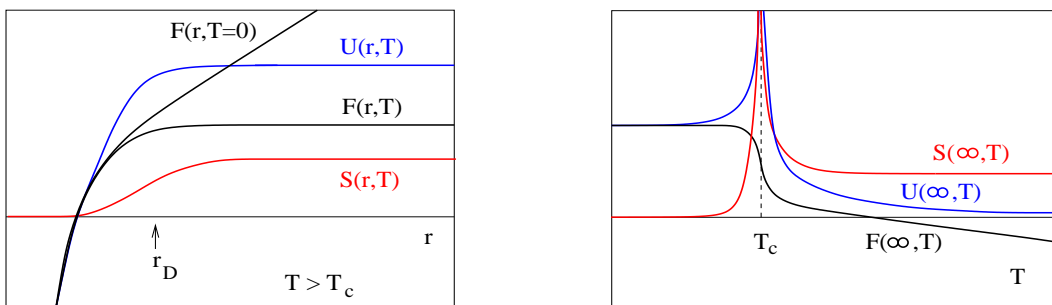


Figure 10: Thermodynamic potentials as function of r and T

For a quantitative potential theory study, we now have to extract the in-medium heavy quark potential $V(r, T)$ from the color singlet internal energy obtained in lattice QCD. It

appears that so far this task is not solved in an unambiguous way, in spite of a number of attempts. We therefore summarize these and their results, indicating the remaining problems.

The internal energy U is the expectation of the Hamiltonian \mathcal{H} , in our case the difference in interaction energy between a system with and one without the heavy quark pair at rest in the medium. Hence we have

$$U(r, T) = \frac{P^2}{m} + V(r, T), \quad (22)$$

where the first term gives the relative kinetic energy and $V(r, T)$ the interaction potential. The lattice results we want to use are obtained for a static $Q\bar{Q}$ pair, so that there is no relative kinetic energy, and hence $U(r, T)$ is our effective potential. However, at very large separation, the Q and the \bar{Q} do not see each other any more and hence cannot interact. Nevertheless, they will still polarize the medium in their vicinity and thus make $U(\infty, T)$ different from zero. This polarization cloud can be interpreted as an effective heavy quark thermal mass $m(T) \geq m_c$. Near T_c , the gluonic correlation length becomes very large (or even diverges), thus increasing the size of the clouds. It is this effect which causes the dramatic increase in $U(\infty, T)$ as T approaches T_c (see the right part of Fig. 10). As the Q and the \bar{Q} get closer to each other, the polarization clouds begin to overlap and hence interact. The interaction enhances the binding potential between the two heavy quark components, and this cloud-cloud interaction is what leads $U(r, T)$ near r_D to overshoot the $T = 0$ form. The free energy does not contain this component and hence approaches the Cornell potential. For a further discussion, see [25].

The relevant Schrödinger equation thus becomes

$$\left\{ 2m_c - \frac{\nabla^2}{m_c} + U(r, T) \right\} \Phi_i(r, T) = M_i(T) \Phi_i(r, T), \quad (23)$$

and the resulting dissociation temperatures are listed in Table 4. As we shall see shortly, they agree quite well with the values presently quoted in lattice studies. However, the inclusion of the cloud-cloud interaction has been put to question, and so the Schrödinger equation has also been solved with potentials of an intermediate form $V(r, T; x) = x U(r, T) + (1 - x) F(r, T)$, with $0 \leq x \leq 1$. The results tend towards those of Table 4 for $x \rightarrow 1$ and give lower dissociation temperatures as $x \rightarrow 0$ [26–28].

state	$J/\psi(1S)$	$\chi_c(1P)$	$\psi'(2S)$	$\Upsilon(1S)$	$\chi_b(1P)$	$\Upsilon(2S)$	$\chi_b(2P)$	$\Upsilon(3S)$
T_d/T_c	2.10	1.16	1.12	> 4.0	1.76	1.60	1.19	1.17

Table 4: Quarkonium Dissociation Temperatures [9]

We thus have to conclude that at this time, a final answer is still not provided in the potential study approach. Besides the mentioned potential ambiguities, a further difficulty shared by all potential models is that the dissociation points are defined as those temperature values for which the diameter r_i of a given state i diverges (see Fig. 11). As seen, this leads to “bound state” regions in which $r_i \gg T^{-1}$ and in fact surpasses the normal hadronic size r_h . One may expect [29] that under such conditions, thermal dissociation will break up any bound state, so that the actual bound state survival ends when its radius reaches the size of the screening radius [30].

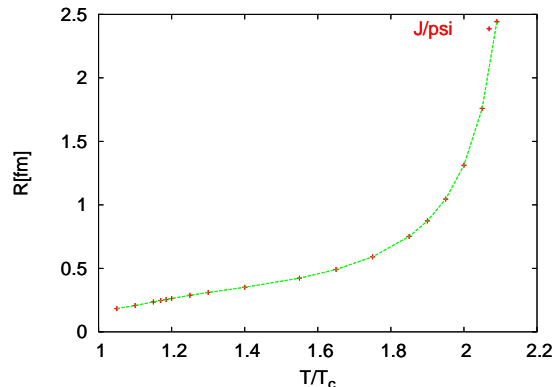


Figure 11: T -dependence of the bound state diameter for the J/ψ [9]

3.3 Charmonium Correlators

The direct spectral analysis of charmonia in finite temperature lattice has come within reach only in very recent years [31–36]. It is possible now to evaluate the correlation functions $G_i(\tau, T)$ for charmonium quantum number channels i in terms of the Euclidean time τ and the temperature T . These correlation functions are directly related to the corresponding spectral function $\sigma_i(M, T)$,

$$G_i(\tau, T) = \int d\omega \sigma_i(\omega, T) K(\omega, \tau, T), \quad (24)$$

which describe the distribution in mass M at temperature T for the channel in question. Here the kernel

$$K(\omega, \tau, T) = \frac{\cosh[\omega(\tau - (1/2T))]}{\sinh(\omega/2T)} \quad (25)$$

provides the relation between the imaginary time τ and the $c\bar{c}$ energy ω . The inversion of eq. (24) with the help of the maximum entropy method (MEM) provides the desired spectrum [37]. In Fig. 12, schematic results at different temperatures are shown for the J/ψ and the χ_c channels. It is seen that the spectrum for the ground state J/ψ remains essentially unchanged even at $1.5 T_c$. At $3 T_c$, however, it has disappeared; the remaining spectrum is that of the $c\bar{c}$ continuum of J/ψ quantum numbers at that temperature. In contrast, the χ_c is already absent at $1.1 T_c$, with only the corresponding continuum present.

These results are very promising: they indicate that in a foreseeable future, the dissociation parameters of quarkonia can be determined *ab initio* in lattice QCD. After first calculations performed in quenched QCD [31–35], i.e., without dynamical quark loops, there now are also results from two-flavor QCD [36], and these fully support the late dissociation of the J/ψ . The widths of the observed spectral signals are at present determined by the precision of the lattice calculations; to study the actual physical widths, much higher precision is needed. Moreover, one has so far only first signals at a few selected points; a temperature scan also requires higher performance computational facilities. Since the next generation of computers, in the multi-Teraflops range, is presently going into operation, the next years should bring the desired results.

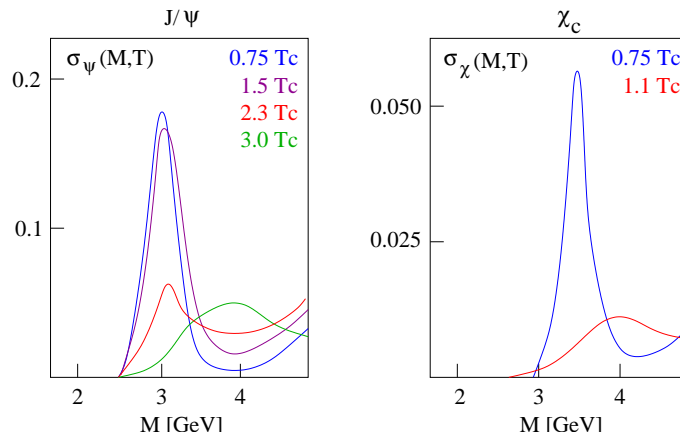


Figure 12: J/ψ and χ_c spectral functions at different temperatures

So far, in view of the mentioned uncertainties in both approaches, the results from direct lattice studies and those from the potential model calculations of the previous section appear compatible. We note at this point, however, that numerous attempts to obtain information on charmonium survival by comparing the calculated correlator to reference correlators constructed from models of low or zero temperature spectra and relating the results to potential studies [38–40] have so far not really provided unambiguous information. Hence further work on the theory of in-medium charmonium behavior, in lattice studies as well as in analytic approaches [41–45], is clearly called for.

4 Charmonium Production in Hadronic Collisions

4.1 Elementary Collisions

The hadroproduction of charmonia occurs in two stages. The first stage is the production of a $c\bar{c}$ pair; because of the large quark mass, this process is well described by perturbative QCD (Fig. 13). A parton from the projectile interacts with one from the target; the (non-perturbative) parton distributions within the hadrons are determined empirically in other reactions, e.g. by deep inelastic lepton-hadron scattering. The produced $c\bar{c}$ pair is in general in a color octet state. In the second stage, it neutralises its color and then eventually forms physical resonances, such as J/ψ , χ_c or ψ' . Color neutralisation occurs by interaction with the surrounding color field; this and the subsequent resonance binding are presumably of non-perturbative nature.

On a fundamental theoretical level, color neutralization is not yet fully understood. However, the color evaporation model [46] provides a simple and experimentally well-supported phenomenological approach. In the evaporation process, the c and the \bar{c} can either combine with light quarks to form open charm mesons (D and \bar{D}) or bind with each other to form a charmonium state. The basic quantity in this description is the total sub-threshold charm cross section $R_{c\bar{c}}$, obtained by integrating the perturbative $c\bar{c}$ production cross section σ over the mass interval from $2m_c$ to $2m_D$. At high energy, the dominant part of $R_{c\bar{c}}$

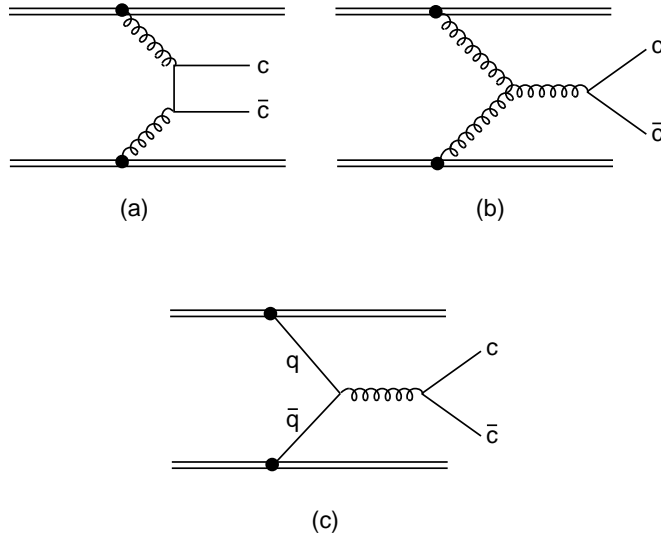


Figure 13: Lowest order diagrams for $c\bar{c}$ production in hadronic collisions, through gluon fusion (a,b) and quark-antiquark annihilation (c).

comes from gluon fusion (Fig. 13a), so that we have

$$R_{c\bar{c}}(s) \simeq \int_{2m_c}^{2m_D} d\hat{s} \int dx_1 dx_2 g_P(x_1) g_T(x_2) \sigma(\hat{s}) \delta(\hat{s} - x_1 x_2 s), \quad (26)$$

with $g_P(x)$ and $g_T(x)$ denoting the gluon densities [47], x_1 and x_2 the fractional momenta of gluons from projectile and target, respectively; σ is the $gg \rightarrow c\bar{c}$ cross section. In pion-nucleon collisions, there are also significant quark-antiquark contributions (Fig. 13c), which become dominant at low energies. The basic statement of the color evaporation model is that the production cross section of any charmonium state i is a fixed fraction of the subthreshold charm cross section,

$$\sigma_i(s) = f_i R_{c\bar{c}}(s), \quad (27)$$

where f_i is an energy-independent constant to be determined empirically. It follows that the energy dependence of the production cross section for any charmonium state is predicted to be that of the perturbatively calculated sub-threshold charm cross section. As a further consequence, the production ratios of different charmonium states

$$\frac{\sigma_i(s)}{\sigma_j(s)} = \frac{f_i}{f_j} = \text{const.} \quad (28)$$

must be energy-independent. Both these predictions have been compared in detail to charmonium and bottomonium hadroproduction data over a wide range of energies [48]; they are found to be well supported, both in the energy dependence of the cross sections and in the constancy of the relative species abundances. Let us consider in more detail what this tells us about the hadronization of charm quarks.

We recall that the relative abundances of light hadrons produced in hadron-hadron and e^+e^- interactions follow the statistical pattern governed by phase space weights [49, 50]:

the relative production rates are those predicted by an ideal resonance gas at the confinement/deconfinement transition temperature $T_c \simeq 175$ MeV. For two hadron species i and j that implies at all (high) collision energies

$$R_{i/j} \simeq \frac{d_i}{d_j} \left(\frac{m_i}{m_j} \right)^{3/2} \exp -\{(m_i - m_j)/T_c\} \quad (29)$$

for the ratio of the production rates, with d_i for the degeneracy (spin, isospin) and m_i for the mass of species i . For strange particles, the rates (29) overpredict the experimental data; this can, however, be accommodated by a common strangeness suppression factor $\gamma_s \simeq 0.5 - 0.7$, applied as γ_s^n if the produced hadron contains n strange quarks [51]. A recent alternative explanation for strangeness abundances is based on the assumption of a color event horizon with corresponding Unruh radiation [52].

For the hadroproduction of charm, such a statistical description does not work, as seen in three typical instances [48, 53]:

- The total $c\bar{c}$ cross section increases with energy by about a factor ten between $\sqrt{s} = 20$ and 40 GeV, while the light hadron multiplicity only grows by about 20%. Hence the ratios of hadrons with and without charm are not energy-independent.
- From $p - p$ data one finds for J/ψ production a weight factor $f_{J/\psi} \simeq 2.5 \times 10^{-2}$. Since the subthreshold $c\bar{c}$ cross section is about half of the single D production cross section [53], this implies $R_{(J/\psi)/D} \simeq 10^{-2}$; the ideal resonance gas gives with $R_{(J/\psi)/D} \simeq 10^{-3}$ a prediction an order of magnitude smaller. Of the total charm production, more goes into the hidden charm sector than statistically allowed.
- For the production ratio of ψ' to J/ψ , which have the same charm quark infrastructure, one finds experimentally over a wide range of collision energies $R_{\psi'/(J/\psi)} \simeq 0.23$. This energy-independent ψ' to J/ψ ratio can be accounted for in terms of the charmonium masses and wave functions; it disagrees strongly with the statistical prediction, which gives with $R_{\psi'/(J/\psi)} \simeq 0.045$ a very much smaller value. The same holds true for the other measured charmonium states [9].

Charm production in elementary collisions thus does not seem to be of statistical nature. It appears to be determined by parton dynamics at an early stage [54], rather than by the phase space size at the confinement temperature.

Although the color evaporation model provides a viable phenomenological description of the hadroproduction of quarkonia, leading to correct quantitative predictions up to the highest energies under consideration, it cannot predict the fractions f_i of the hidden charm cross sections, and it can even less describe the space-time evolution of color neutralization. For charmonium production in p-A and A-B collisions, the latter is crucial, however, and hence a more detailed description of color neutralization is needed.

In the first step of the collision process, a $c\bar{c}$ pair is formed through a hard process, with very short formation time $\tau_{c\bar{c}}$; to reach subsequently J/ψ quantum numbers, the $c\bar{c}$ must be in a color octet state. The color octet model [55] proposes that this $c\bar{c}$ then combines with a soft collinear gluon to form a color singlet ($c\bar{c}-g$) state. After a relaxation time τ_8 , this pre-resonant ($c\bar{c}-g$) state turns into the physical $c\bar{c}$ mode by absorbing the accompanying gluon, with similar formation processes for χ_c and ψ' production. The color octet

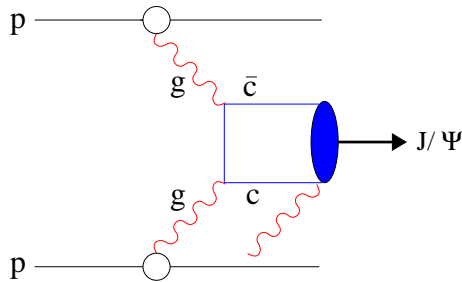


Figure 14: The evolution of J/ψ production

model encounters difficulties if the collinear gluons are treated perturbatively, illustrating once more that color neutralization seems to require non-perturbative elements [56, 57]. However, it does provide a conceptual basis for the evolution of the formation process (see Fig. 14). The color neutralization time τ_8 of the pre-resonant state can be estimated [58]; it is essentially determined by the lowest momentum possible for confined gluons, $\tau_8 \simeq (2m_c\Lambda_{\text{QCD}})^{1/2} \simeq 0.25$ fm. The resulting scales in J/ψ formation are illustrated in Fig. 15. The formation time for the actual physical ground state J/ψ is presumably somewhat larger than τ_8 ; although $r_{J/\psi}/2 \simeq \tau_8$, the heavy c quarks do not move with the velocity of light. For the larger higher excited states, the formation times will then be correspondingly larger.

	0.05 fm	0.25 fm
hard	pre-resonance	resonance
$\tau_{c\bar{c}} = 1/2m_c$	$\tau_8 = 1/\sqrt{2m_c\Lambda_{\text{qcd}}}$	

Figure 15: Scales of J/ψ production

There is one further important feature to be noted for J/ψ hadroproduction. The J/ψ 's actually measured in hadron-hadron collisions have three distinct origins: about 60 % are directly produced 1S charmonium states, while about 30 % come from the decay $\chi_c(1P) \rightarrow J/\psi + \text{anything}$, and the remaining 10 % from $\psi'(2S) \rightarrow J/\psi + \text{anything}$ [59]. Such feed-down also occurs in Υ production [60]. In all cases, the decay widths of the involved higher excited states are extremely small (less than one MeV), so that their lifetimes are very long. The presence of any medium in nuclear collisions would therefore affect these excited states themselves, and not their decay products.

4.2 $p - A$ Collisions

In $p - A$ collisions, the presence of normal nuclear matter can affect charmonium production, so that such collisions provide a tool to probe the effect of confined matter. Nuclear effects can arise during the entire evolution of J/ψ production, and several different phenomena have been studied in considerable detail. We note in particular:

- The presence of other nucleons in the nucleus can modify the initial state parton distribution functions, which enter in the perturbative $c\bar{c}$ production process illustrated in Fig. 13.

- Once it is produced, the $c\bar{c}$ pair can be dissociated in the pre-resonance as well as in the resonance stage, due interactions with nucleons during its passage through the target nucleus.

In both cases, the crucial quantity is the momentum of the charmonium state as measured in the nuclear target rest frame.

Since we eventually want to probe the effect which the ‘secondary’ medium *produced* by nucleus-nucleus collisions has on charmonium production, it is of course essential to account correctly for any effects of the nuclear medium initially present. Let us therefore first summarize the main features observed for charmonium production in $p - A$ collision experiments [62].

- At fixed collision energy, quarkonium production rates per target nucleon decrease with increasing A .
- The production rates decrease for increasing J/ψ momentum as measured in the nuclear target rest frame.
- The nuclear reduction at $p - N$ mid-rapidity appears to become weaker with increasing collision energy.
- For fixed collision energy, mass number A and J/ψ rapidity, the reduction appears to increase with the centrality of the collision.
- At sufficiently high momentum in the target rest frame, the different charmonium states appear to suffer the same amount of reduction, while at lower energy, the ψ' is affected more than the J/ψ .

At present, there does not seem to exist a theoretical scenario able to account quantitatively for all these observations. In fact, so far not even a common scaling variable for the different effects has been found. Shadowing would suggest scaling in the fractional target parton momentum x_2 , while absorption of the pre-resonance state would point to the fractional beam momentum x_F . Neither is in good accord with the data. The problem has recently been addressed in the context of parton saturation and color glass condensate formation [61]. Here we shall concentrate on indicating some operational methods to specify nuclear effects in $p - A$ collisions in a way that can be extended to $A - B$ collisions; for further discussions, we refer to reviews [62,63]. The problems encountered in formulating a theoretical description of charmonium production on nuclear targets underline again the crucial importance of having $p - A$ data in order to arrive at a correct interpretation of $A - A$ results.

We now return in some more detail to the two main aspects arising for charmonium production in pA collisions, the (initial state) nuclear modification of the parton distribution function and the (final state) absorption of the nascent charmonium state during its traversal of the nucleus.

Assuming again gluon fusion as the dominant high energy process of $c\bar{c}$ formation, we have for J/ψ production in pA collisions (see eqs. (26) and (27))

$$R_{J/\psi}(s) \simeq f_{J/\psi} \int_{2m_c}^{2m_D} d\hat{s} \int dx_1 dx_2 g_p(x_1, \mu^2) g_A(x_2, \mu^2) \sigma(\hat{s}) \delta(\hat{s} - x_1 x_2 s), \quad (30)$$

where μ denotes the scale of the probe in the evaluation of the gluon distribution functions in either the proton (g_p) or the nucleus (g_A). The nuclear modification of the distribution functions have been studied in detail in different approaches [64]. In Fig. 16 we show a typical result for the ratio $R_A^g(x)$ of the gluon distribution function of a nucleon in a heavy nucleus, relative to that in a single nucleon. It is shown as function of the Bjorken variable x , specifying the fraction of the nucleon momentum carried by the gluon. We note that there are essentially four different regimes. Near $x = 1$, Fermi motion inside the nucleus leads to an enhancement; following this is a suppression (the EMC effect) due to nucleon-nucleon interactions. Around $x \simeq 0.1$, we then again have an enhancement (“anti-shadowing”), followed by a suppression at very small x (“shadowing”). High energy collisions generally access regions $x \leq 0.1$, so that anti-shadowing and shadowing are the phenomena of particular interest. Depending on the collision energy and the momentum of the observed J/ψ , the production rate can thus be either enhanced or reduced by the initial state nuclear modification of the gluon distribution function. In order to determine the effect of the final state (cold nuclear matter or, in AA collisions, a possible QGP) on charmonia, such initial state modifications must evidently be brought under control.

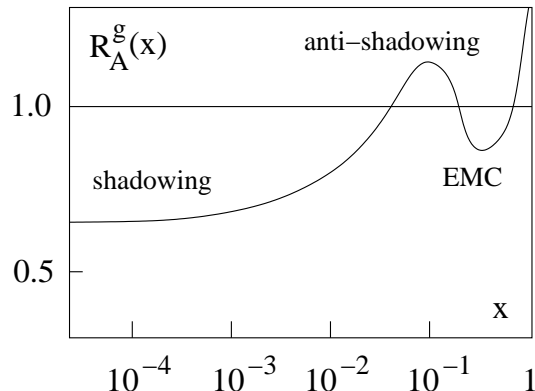


Figure 16: Nuclear modifications of the gluon distribution function

The second aspect is the dissociation of the nascent J/ψ in cold nuclear matter; the $c\bar{c}$ pair has thus been formed, with whatever nuclear modifications of the parton distribution functions applied for its formation rate, and now traverses the remaining part of the nucleus. To specify the dissociation, we note [66] that according to the Glauber formalism of nuclear scattering theory, a $c\bar{c}$ pair formed at point z_0 in a target nucleus A has a survival probability

$$S_i^A = \int d^2b dz \rho_A(b, z) \exp \left\{ -(A-1) \int_{z_0}^{\infty} dz' \rho_A(b, z') \sigma_{\text{diss}}^i \right\}, \quad (31)$$

where the integration covers the path, at impact parameter b , remaining from z_0 out of the nucleus, and where σ_{diss}^i describes the overall “absorption” effect on the observed charmonium state i along the path. The result is then averaged over impact parameter and path lengths. The traversed medium of nucleus A is parametrized through a Woods-Saxon density distribution $\rho_A(z)$, and by comparing S_i to data for different targets A , the effective dissociation cross section can be obtained for the J/ψ and ψ' absorption in nuclear matter. The effect of the charmonium passage through the nucleus will arise from

a superposition of the different stages; but if part of the passage is carried out as physical resonance, higher excited states should lead to larger absorption cross-sections than the much smaller ground state J/ψ .

The way charmonium production in pA (or dA) collisions enters the analysis is thus clear: with the initial state modifications of the parton distribution functions taken into account, the dissociation cross section in cold nuclear matter has to be determined. With this given as a baseline, one can then turn to AA collisions and look for the effects of a newly produced medium.

It should be noted here that in some studies [66] the initial and final state effects have been parametrized jointly in the form of a common “dissociation cross-section”, which includes both sources of modification. With the help of this cross section, normal nuclear matter effects were then calculated for nucleus-nucleus collisions. Evidently such a procedure makes sense only if neither of the nuclear modifications depend sensitively on the momentum of produced charmonium state, or if the accessible momentum range is the same and very small both in $p - A$ and in nuclear collisions. For the SPS data, the latter seems to be the case.

4.3 Nuclear Collisions

The basic assumption in the attempt to create deconfined matter through nuclear collisions is that the excited vacuum left after the passage of the colliding nuclei forms a thermal medium. This picture is schematically illustrated in Fig. 17. A charmonium state produced in such a collision will in its early stages first be subject to the possible effects of the nuclear medium, just as it is in $p - A$ collisions, and then, after the nuclei have separated, encounter the newly produced medium.

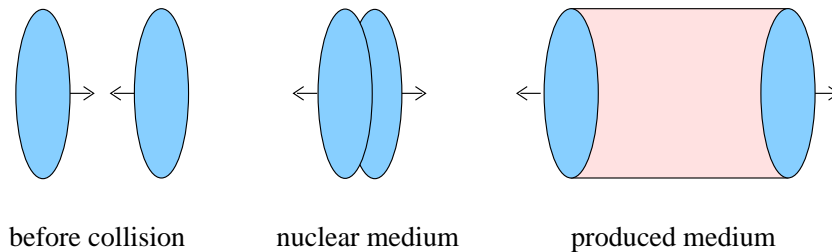


Figure 17: Collision stages

The Glauber formalism used above to calculate the survival probability of an evolving charmonium state in a $p - A$ collision now has to be extended to $A - B$ interactions [66]. The survival probability at impact parameter b now becomes

$$S_i^{AB}(b) = \int d^2s dz dz' \rho_A(s, z) \rho_B(b - s, z') \times \exp \left\{ -(A - 1) \int_{z_0^A}^{\infty} dz_A \rho_A(s, z_A) \sigma_{diss}^i - (B - 1) \int_{z_0^B}^{\infty} dz_B \rho_B(b - s, z_B) \sigma_{diss}^i \right\}, \quad (32)$$

as extension of Eq. (31). Here z_0^A specifies the formation point of the $c\bar{c}g$ within nucleus A , z_0^B its position in B . With the dissociation cross sections σ_{diss}^i determined in $p - A$ collisions, Eq. (32) specifies the ‘normal’ survival probability, i.e., that due to only the nuclear medium.

To use quarkonia as probes for the produced medium, we now have to study how the behavior observed in $A - A$ collisions differs from this predicted pattern. Several possible and quite different effects have been considered as consequences of the produced medium on charmonium production.

- **Suppression by comover collisions:** A charmonium state produced in a primary nucleon-nucleon collision can be dissociated through interactions with the constituents of any medium subsequently formed in the collision. Such dissociation could in principle occur in a confined [70] as well as in a deconfined medium [10].
- **Suppression by color screening:** If the produced medium is a hot QGP, it will dissociate by color screening the charmonium states produced in primary nucleon-nucleon collisions [1]. Since the different states have different dissociation temperatures, a sequential suppression pattern will specify the relevant thresholds [4, 5, 71].
- **Enhancement by regeneration:** In the hadronization stage of the QGP, charmonium formation could occur through the binding of a c with a \bar{c} from different nucleon-nucleon collisions. If the total number of available $c\bar{c}$ pairs considerably exceeds their thermal abundance, such statistical regeneration could enhance hidden relative to open charm production, as compared to hadron-hadron collisions [72–75].

In addition, the partonic initial state of the colliding nuclei, which leads to the formation of the produced medium and to that of charmonium states, will change its nature for large A and sufficiently high \sqrt{s} ; eventually, parton percolation (saturation or color glass formation) can lead to a very different medium, with possible effects on production and binding of charmonia [76].

Is it possible for experiment to distinguish between these different scenarios? Before turning to the experimental situation, we want to discuss in some more detail the salient features of each approach.

4.3.1 Suppression by Comover Collisions

If the charmonium state moves in a random scattering pattern through the produced medium, its survival rate is approximately given by

$$S_i = \exp\{-\sigma_i n \tau_0 \ln[n/n_f]\} \quad (33)$$

with σ_i denoting the dissociation cross section, n the initial density of the medium after a formation time τ_0 , and n_f the ‘freeze-out’ density, at which the interactions stop.

Since the cross section for J/ψ break-up through gluon collisions is large [10] and the gluon density high, there will be significant charmonium suppression in a deconfined medium, even if this is not thermalized. In an equilibrium QGP, this dissociation is presumably

accounted for by color screening, provided the effect of the medium on the width of the surviving states is also calculated.

Charmonium dissociation by interaction with hadronic comovers has received considerable attention in the past [70]. However, if one restricts the possible densities to values appropriate to hadronic matter ($n_h \lesssim 0.5 \text{ fm}^{-3}$) and the cross sections to those obtained in section 3, the effect of hadron dissociation is negligible. Even a cross section increase to the high energy limit still leads to less than 10% effects. More recent analyses [77] thus conclude that a hadronic medium will not result in significant suppression.

In Fig. 18 we illustrate schematically the overall behavior expected for J/ψ dissociation through comover collisions, assuming that beyond a deconfinement threshold, the comover density increases with energy density in a monotonic fashion, with little or no prior suppression in the hadronic regime.

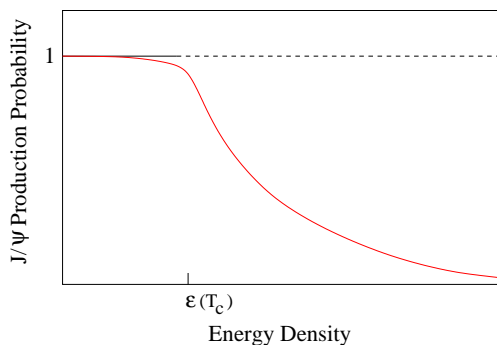


Figure 18: J/ψ suppression by comover collisions

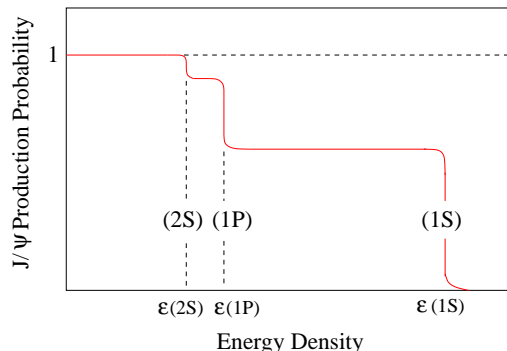


Figure 19: Sequential J/ψ suppression by color screening

4.3.2 Suppression by Color Screening

The theoretical basis of this effect has been considered in detail in chapters 3 and 4; the color field between the heavy quarks becomes modified due to the presence of a medium of unbound color charges. The results obtained for this effect in statistical QCD are as such model-independent, once all calculational constraints are removed. What is speculative and model-dependent is its application to nuclear collisions: these do not necessarily produce the medium studied in thermal QCD, and the different evolution stages in nuclear collisions can introduce factors not present in the study of equilibrium thermodynamics, such as the oversaturation of $c\bar{c}$ pairs just mentioned.

If the medium produced in high energy nuclear collisions is indeed the quark-gluon plasma of statistical QCD, and if charmonium production can be treated as a distinct process within such an environment, then the effect of color screening seems clear. The partitioning of the $c\bar{c}$ pairs produced in nucleon-nucleon collisions into hidden and open charm is non-statistical, favouring the hidden charm sector because of dynamical binding effects. Color screening destroys these and hence strongly suppresses charmonium production rates relative to those observed in elementary interactions.

A crucial feature of J/ψ suppression by deconfinement is its sequential nature [5, 30, 71, 78]. In the feed-down production of J/ψ , the produced medium affects the intermediate excited states, so that with increasing temperature or energy density, first the J/ψ 's originating from ψ' decay and then those from χ_c decay should be dissociated. Only considerably higher temperatures would be able to remove the directly produced J/ψ 's. Such a stepwise onset of suppression, with specified threshold temperatures, is perhaps the most characteristic feature predicted for charmonium as well as bottomonium production in nuclear collisions. It is illustrated schematically in Fig. 19, where we have defined the J/ψ production probability to be unity if the production rate suffers only the calculated nuclear suppression.

4.3.3 Enhancement through Regeneration

In charmonium hadroproduction, J/ψ 's are formed because some of the $c\bar{c}$ pairs produced in a given collision form a corresponding bound state. In a collective medium formed through superposition of many nucleon-nucleon (NN) collisions, such as a quark-gluon plasma, a c from one NN collision can in principle also bind with a \bar{c} from another NN collision. This ‘exogamous’ charmonium formation at a later evolution stage could lead to enhanced J/ψ production, provided the overall charm density of the medium at hadronization is sufficiently high and provided the binding force between charm quarks from different sources is large enough [72–74].

The production of $c\bar{c}$ pairs in primary collisions is a hard process and thus grows in $A - A$ interactions with the number of nucleon-nucleon collisions; in contrast, the multiplicity of light hadrons grows roughly as the number of participant nucleons. Hence the relative abundance of charm to non-charm quarks will be higher in $A - A$ than in $p - p$ collisions. Moreover, the $c\bar{c}$ production cross section increases faster with energy than that for light hadron production. The two effects together imply that in the medium produced in energetic $A - A$ collisions, the ratio of charm to non-charm quarks is initially much higher than in an equilibrated QGP. Whether or not this results in a charmonium regeneration depends on two factors. On one hand, the initial charm oversaturation must be preserved, so that the total charm abundance is non-thermal. On the other hand, it is necessary that the binding potential of random pairs into charmonia is sufficiently strong.

Charmonium regeneration in nuclear collisions will be addressed in a separate section of this Handbook [75]. We only note here that several studies have led to considerable enhancement factors [75, 79], in the strongest form even predicting a large overall enhancement of J/ψ production in $A - A$ collisions relative to $p - p$ results scaled by binary collisions. One crucial prediction of the approach is the *increase* of the enhancement with centrality, as shown in Fig. 20, because of the corresponding increase in the number of collisions and hence of the number of $c\bar{c}$ pairs. Another is that the distributions of the observed charmonia in transverse momentum as well as in rapidity must be given as convolutions of the open charm distributions [80]. What this means for transverse momentum spectra will be addressed in the next subsection.

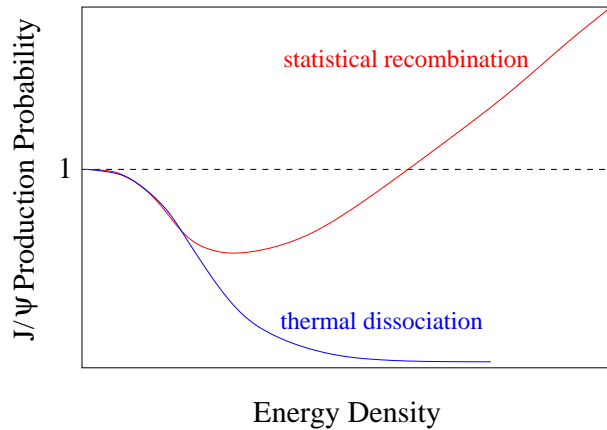


Figure 20: J/ψ enhancement by statistical regeneration

4.4 Transverse Momentum Behavior

The production pattern of charmonia as function of their transverse momentum can provide information about the production process, the evolution of the resonance formation and of that of the produced medium. We begin with the production process.

The transverse momentum distribution of charmonia measured in pA as well as in AA collisions is generally broadened in comparison to that in pp interactions. The main effect causing this is the collision broadening of the incident gluons which fuse to make $c\bar{c}$ pairs. A standard random walk analysis gives for the squared transverse momentum of the produced J/ψ [81,82]

$$\langle p_T^2 \rangle_{pA} = \langle p_T^2 \rangle_{pp} + N_c^A \delta_0 \quad (34)$$

in $p-A$ and to

$$\langle p_T^2 \rangle_{AA} = \langle p_T^2 \rangle_{pp} + N_c^{AA} \delta_0 \quad (35)$$

in $A-A$ collisions. Here N_c^A denotes the average number of collisions of a projectile parton in the target nucleus A , and N_c^{AA} the sum of the average number of collisions of a projectile parton in the target and vice versa, at the given centrality. The parameter δ_0 specifies the average “kick” which the incident parton receives in each subsequent collision. The crucial parameters are thus the elementary $\langle p_T^2 \rangle_{pp}$ from $p-p$ interactions and the value of δ_0 , determined by corresponding $p-A$ data; both depend on the collision energy. The A -dependence of N_c^A as well as the behavior of N_c^{AA} as function of centrality can be obtained through a Glauber analysis including absorption in cold nuclear matter, thus specifying the “normal” centrality dependence of $\langle p_T^2 \rangle_{AA}$. In the absence of any anomalous suppression, this would be the expected behavior of the average J/ψ transverse momentum.

Given the sequential suppression by color screening, the J/ψ 's observed for energy densities in a range above the onset of anomalous suppression, $\epsilon(2S), \epsilon(1P) \leq \epsilon \leq \epsilon(1S)$ are the directly produced $1S$ states unaffected by the presence of the QGP. They should therefore still show the normal broadening pattern (35), increasing linearly with the number of collisions as long as $\epsilon < \epsilon(1S)$ [71]. This broadening is a memory of the initial state and hence essentially absent if the J/ψ is formed only at the hadronization point, where such

memory has been destroyed. Thus J/ψ production through regeneration should show a flat distribution as function of the number of collisions [80], in contrast to the rise expected in the sequential suppression scenario. The behavior of $\langle p_T^2 \rangle_{AA}$ thus should provide a clear indication of how the observed J/ψ 's were produced. In Fig. 21 we illustrate the different patterns expected.

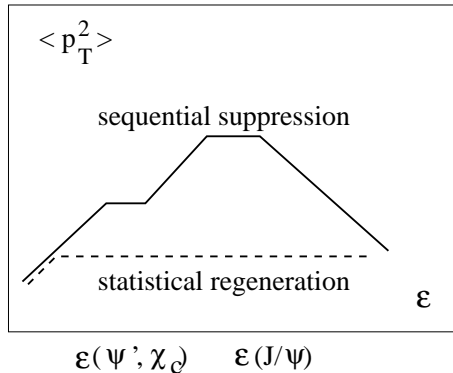


Figure 21: Transverse momentum broadening in sequential suppression vs. statistical regeneration scenarios

A further interesting signal is how an anomalous suppression behaves as function of p_T . If the nascent J/ψ is formed as a small color singlet gradually expanding to its physical size, then it can be out of the deconfining medium either spatially [83] or temporally [84] before suffering serious suppression, provided it has a high enough transverse momentum. The “end” of anomalous suppression as function of p_T could thus give indication on the size or life-time of the QGP.

More recently, calculations have appeared [85] which are based on the AdS/CFT correspondence applied to QCD; they indicate the opposite effect, suggesting that J/ψ 's of high transverse momentum should suffer more suppression. It must be kept in mind, however, that binding and the dissociation of specific bound states are clearly non-conformal phenomena, so that such modelling is not necessarily valid.

5 Summary of the Theoretical Status

The theoretical work of the past years has done much to clarify the questions that must be answered in order to reach final conclusions.

In statistical QCD, improved MEM techniques, better statistics (from faster computers) as well as larger lattices (on larger computers), promise that in the foreseeable future we will have reliable first principle calculations of the in-medium behavior of quarkonia.

These will hopefully then be related to the results from heavy quark studies in finite temperature lattice QCD. In this work (see e.g. [16,17,86]), there are at present still several unsolved questions, concerning in particular gauge invariance and the specification of specific color states, and the possible in-medium transitions between color states. Recent analytical work may provide help in dealing with them [42–45].

In parallel, potential theory studies are expected to provide further insight into the melting of quarkonia in a hot QGP. One of the basic issues to be addressed here is if and how the multi-component problem near T_c can be addressed. In particular, the role of the gluonic dressing in heavy quark binding has to be taken into account [87].

Once the in-medium behavior of quarkonia is clarified in statistical QCD, one can hope to address the behavior observed in high energy nuclear collisions. If these indeed produce a QGP in the sense of statistical QCD, sequential melting threshold could provide a direct quantitative connection between theory and experiment. If, on the other hand, the measured quarkonia are largely due to regeneration at hadronization, i.e., to the combination of secondary Q and \bar{Q} from different nucleon-nucleon interactions, it is not evident how such a connection can be obtained. It would, however, provide clear evidence for the production of a deconfined thermal medium.

II Experiment

1 Charmonium Experiments at the CERN-SPS

At the CERN-SPS, experiments NA38, NA50 and NA51 have systematically measured charmonium production with incident protons, Oxygen, Sulphur and Lead beams at various incident momenta. The latest version of the detector [88] was based on a muon pair spectrometer able to stand high intensity incident beam fluxes. The spectrometer was further equipped with three devices leading to three independent estimates of the centrality of the collision. The Electromagnetic Calorimeter measured E_T , the integrated flux of neutral transverse energy, mainly due to neutral pions produced in the collision. The Zero Degree Calorimeter measured E_{ZDC} , the forward energy carried by the beam spectator nucleons. The Multiplicity Detector counted the charged particles produced in the reaction. All these three measurements are related to the impact parameter of the collision.

The properties of the detectors allowed the collection of large samples of data with incident protons and ions. This, in turn, made possible the study of both J/ψ and ψ' production with minimal systematic uncertainties, thanks to the simultaneous detection of Drell-Yan events which could be used as appropriate "debiasing" tools.

From the very beginning, it was taken for granted that the study of J/ψ production from different nuclear targets would provide, by some kind of extrapolation, the appropriate reference baseline, i.e., the "normal" charmonium behavior, relative to which the heavy ion collision specific features would be easily identifiable. Ideally, the reference data would have had to be collected with proton beams of the same energy of that of the

corresponding ion beams, namely 200 GeV, the energy of the Oxygen and Sulphur beams, and later 158 GeV, the energy of the Lead and Indium beams. For low cross-section measurements like charmonium production, it was highly desirable that proton beams be primary beams, directly extracted from the accelerator. Because of various reasons, low energy primary proton beams were not available at CERN. It took 18 years since the start of the heavy ion program until they finally became available, for about 3 days, and could thus be used by experiment NA60.

1.1 The Nuclear Dependence of Charmonium Production

The uncontroversial feature observed since long in charmonium production measurements in $p - A$ reactions is that, at fixed collision energy, quarkonium production rates per target nucleon decrease with increasing A , the target atomic mass number. This effect has been traditionally, and somewhat empirically, quantified with the parametrization $\sigma_{pA} = \sigma_0 \times A^\alpha$ which leads to measured values of α lower than unity. More recently, it has been assumed that some kind of $c\bar{c}$ state is created in the reaction which is dissociated, or rather prevented to finally form a bound state, through interaction with the surrounding nuclear matter. In other words, the $c\bar{c}$ pairs are created proportionally to the number of nucleon-nucleon collisions or, equivalently, to A . Some interact with the surrounding nuclear medium while moving through the target and are no more able to reach a bound state. The final number of charmonium bound states reaching the detector exhibits therefore an apparent suppression with respect to the original A dependence of the $c\bar{c}$ pair production. An appropriate variable to parametrize the measured J/ψ cross-sections should then be the number of nucleons that the created state can potentially interact with [89]. This number can be calculated from the product $\rho \times L$, where ρ is the nuclear density distribution and L the length of nuclear matter the $c\bar{c}$ state traverses while escaping from the interaction region. The charmonium survival probability can then be calculated as a function of an "absorption" or dissociation cross-section σ_{abs} , using the Glauber formalism of nuclear scattering theory or, alternatively, a simplified " ρL " exponential parametrization. Comparison with the experimentally measurable survival probability allows to determine σ_{abs} . As a matter of fact, systematic experiments can even provide some guidance for the validity of this elaborated view of nuclear effects in charmonium production.

Let us underline here that the α parametrization can be used to fit a set of several measurements made under same conditions with different nuclear targets. The procedure then becomes an hypothesis test of such a parametrization. It can also be assumed that nature behaves according to this law and apply the parametrization to only two different targets. The procedure then would just provide an estimate of the numerical value of α , taking for granted that such a parametrization correctly accounts for the elementary process. Identical procedures can be followed under the dissociation cross-section interpretation and resulting parametrization. Finally, let us point out that α and the more elaborated σ_{abs} are obviously correlated.

1.2 Normal Charmonium Production

The first significant samples of charmonium events produced in $p - A$ reactions were collected by experiment NA38 in 1988, with 450 GeV incident protons on various targets. Later on, they were complemented with measurements obtained, as a by-product, from experiment NA51 which provided the data allowing to extract the charmonium production cross-sections for p-p and p-d collisions at 450 GeV [90]. All these data, reanalyzed, with identical procedures as those used to analyze the heavy ion data, led to the production cross-sections plotted in Fig. 1 as a function of the atomic mass number of the target [91].

Some time later, this set of measurements could be complemented with other results from the same experiment NA38, both with protons and with Oxygen and Sulphur beams incident on Copper and Uranium targets, all for collisions at 200 GeV per nucleon. When plotted as a function of the product of the atomic numbers $A \times B$, the comparison of the charmonium production cross-sections at 450 and at 200 GeV exhibits a remarkable feature: the fitted value of α was the same, namely $\alpha_{450}^{J/\psi} = 0.919 \pm 0.015$ and $\alpha_{200}^{J/\psi} = 0.911 \pm 0.034$. The remarkable compatibility of the two values justifies a simultaneous fit of the two sets of points, imposing a single α exponent. This global fit leads to $\alpha^{J/\psi} = 0.918 \pm 0.015$. The observed unexpected agreement between energies and reactions is a serious double hint that nuclear dependence is identical for 450 GeV and for 200 GeV and that, moreover, charmonium production in light ion-induced reactions, namely O-Cu, O-U and S-U, can be considered as normal, namely identical to the one observed in $p - A$ interactions. From the global fit can also be determined the ratio between the values of σ_0 for the 200 and 450 data sets. It amounts to 0.38 ± 0.04 and results from the changes in both \sqrt{s} and in the rapidity domain covered by the two sets of data. The same factor can be used to rescale the 450 GeV ψ' cross-sections to the incident momentum and rapidity range of the 200 GeV data. In fact the ratio between the ψ' and J/ψ production cross-sections in $p - A$ collisions seems to be independent of \sqrt{s} , within the energy domain covered by the currently existing measurements [92]. The J/ψ cross-sections per nucleon-nucleon collision, rescaled if necessary as described above, are shown in Fig. 2. The excellent agreement between the 200 and the 450 GeV results can be easily judged in the case of p-Cu and p-W collision systems for which both measurements exist.

Within the scenario of a dissociation cross-section, its numerical value can also be extracted from the data in the frame of a Glauber calculation. Fig. 3 compares the results, rescaled to 200 GeV and to the 0.0-1.0 rapidity interval, with an overall fit which leads to $\sigma_{\text{abs}} = 7.1 \pm 1.2$ mb. The data exhibit a nice overall agreement with the "Glauber" calculated values and suggest good compatibility with the model, at their level of precision (systematic uncertainties have to be taken into account here). Assuming now the validity of the model, the most precise value of σ_{abs} can be determined using only the 3 most precise measurements, namely p-C, p-Cu and p-W as obtained at 450 GeV. The resulting value obtained from these cross-sections is 5.6 ± 0.4 mb.

The agreement of the Glauber calculation with the experimental data strongly suggests that the A-dependence of J/ψ production can be properly accounted for by final state nuclear absorption up to and including S-U reactions. In particular, there is no indication for any new absorption or dissociation mechanism which would suppress the S-U value

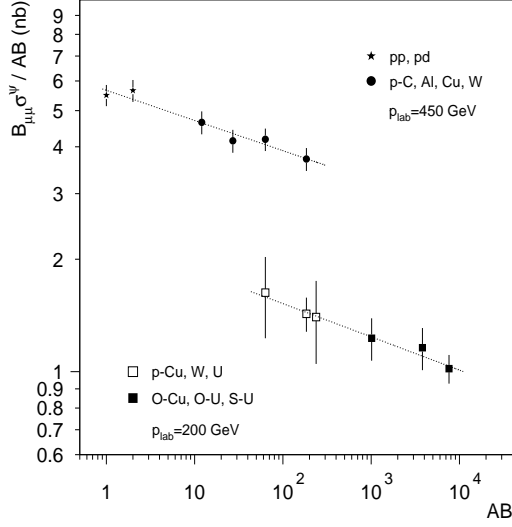


Figure 1: The 450 and 200 GeV J/ψ cross-sections per nucleon (times branching ratio into dimuons, $B_{\mu\mu}$), in the rapidity domain $3.0 < y_{\text{lab}} < 4.0$, as a function of $A \times B$. The lines correspond to the best fit of the function $B_{\mu\mu}^{J/\psi} / (A \times B) = \sigma_0 (A \times B)^{\alpha-1}$.

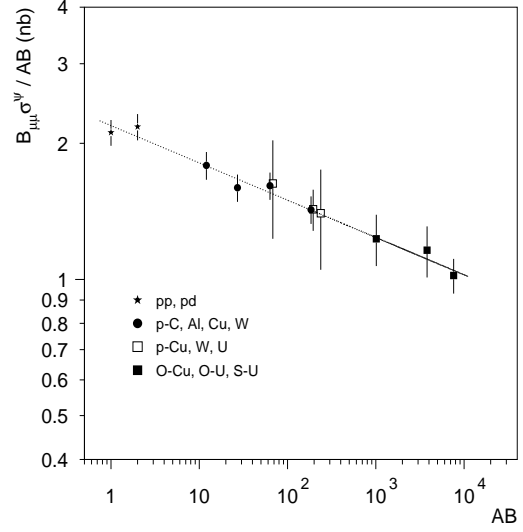


Figure 2: J/ψ cross-sections per nucleon, times b.r., plotted as a function of the product of $A \times B$. The 450 GeV values are here rescaled to 200 GeV and recomputed in the c.m.s. rapidity range 0.0-1.0. The line corresponds to the best fit of the function $B_{\mu\mu}^{J/\psi} / (A \times B) = \sigma_0 (A \times B)^{\alpha-1}$.

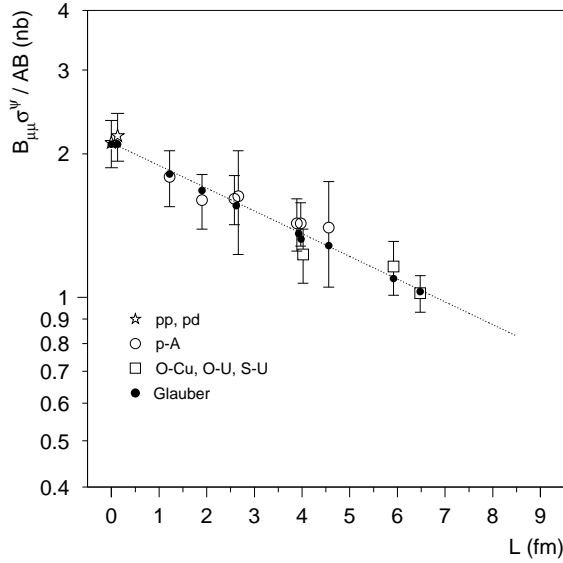


Figure 3: J/ψ cross-sections per nucleon, times b.r., plotted as a function of L . The 450 GeV values are rescaled to the 200 GeV kinematics. The closed circles are the results of the "Glauber" calculation.

relative to the reference baseline established from the p-A systematics.

The same experiments mentioned above did provide the corresponding first results for

ψ' production. Statistical errors, of the order of 10%, were very much too large for precise conclusions. In order to minimize systematic effects, the ratios $\psi' / J/\psi$ measured at 450 GeV in p-C, p-Al, p-Cu and p-W can be considered, as taken under identical experimental conditions and subject to minimal systematic effects with respect to each other. Their values lead to $\alpha^{\psi'} - \alpha^{J/\psi} = -0.060 \pm 0.038$ already suggesting, although within large errors, a normal absorption for ψ' higher than for J/ψ .

In the limited kinematical domain explored by the experiments, the first set of data from experiments NA38 and NA51 led, within their uncertainties, to the following strong indications :

- J/ψ and ψ' are absorbed in nuclear matter.
- For J/ψ , absorption is similar for 450 GeV p-A collisions and for 200 GeV p-A and light ion collisions, up to S-U.
- The absorption is stronger for ψ' than for J/ψ .

Much more precise results obtained later by experiment NA50 allowed to confirm these results both thanks to significantly increased statistics and to a thorough study of systematic uncertainties.

In order to have full control on systematic effects, Drell-Yan muon pairs, always simultaneously measured with charmonium, are the ideal tool despite their significantly lower production cross-section. They allow to use the ratio $J/\psi / \text{Drell-Yan}$, indeed with increased statistical errors but practically free from systematic uncertainties which are usually much more difficult to bring under control. Moreover, they allow with minimal theoretical input the study of nucleus-nucleus collisions as a function of centrality. Indeed, NA50 has proven experimentally that Drell-Yan production is proportional to its theoretically computed value or, equivalently, to the number of nucleon-nucleon collisions, from p-p up to Pb-Pb interactions (Fig. 4). It therefore exhibits no nuclear dependence. The coherent study of the ratio $J/\psi / \text{Drell-Yan}$, both for p-A collisions at 450 GeV (the so-called low intensity (LI) although high statistics sample) and for some p-A and S-U interactions at 200 GeV, the latter as a function of centrality, leads to another estimate of the absorption cross-sections [94]. An independent "Glauber" fit on the S-U ratios gives 6.3 ± 2.9 mb whereas a simultaneous fit to all the data gives 4.3 ± 0.6 mb, as illustrated in Fig. 5. This results further support previous hints that within the errors, no sizable additional suppression mechanism is present in S-U collisions with respect to p-A.

1.3 The First Hints of an Anomaly in Pb-Pb Collisions

The experimental evidence of an unexpected J/ψ suppression resulted from the first Pb-Pb data sample, collected in 1995 [95]. It is illustrated on Fig. 6. The anomalous character results from the comparison of the J/ψ production cross-section per nucleon in Pb-Pb interactions with the assumed *normal* behaviour. The latter, as explained in detail above, was established by simple extrapolation of the behaviour obtained from the "simultaneous" fit method applied to proton and light ion-induced interactions.

The plot should be taken as a strong but only qualitative evidence because of the following *caveat*. The experimental reference is based here on the very first p-A and subsequent

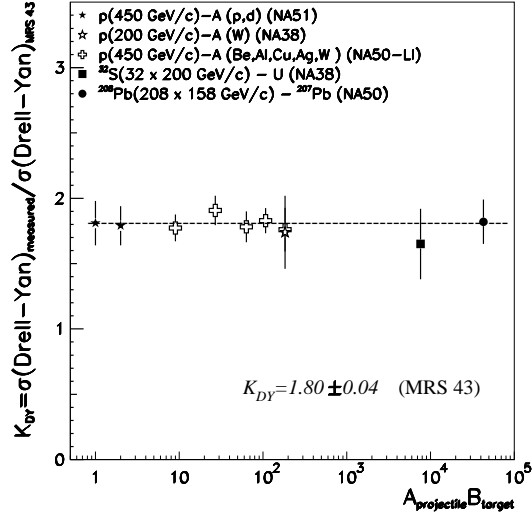


Figure 4: The Drell-Yan "K-factor", as determined experimentally, from p-p up to Pb-Pb interactions (from [93]).

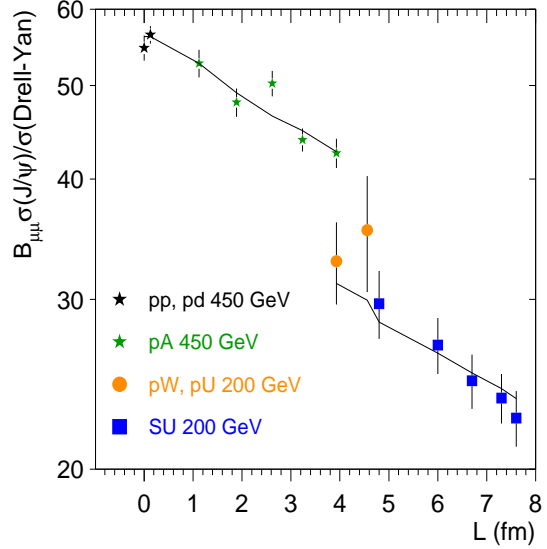


Figure 5: The ratio $B_{\mu\mu} \sigma(J/\psi) / \sigma^{DY}$. The lines are the result of the simultaneous Glauber fit to all the data points.

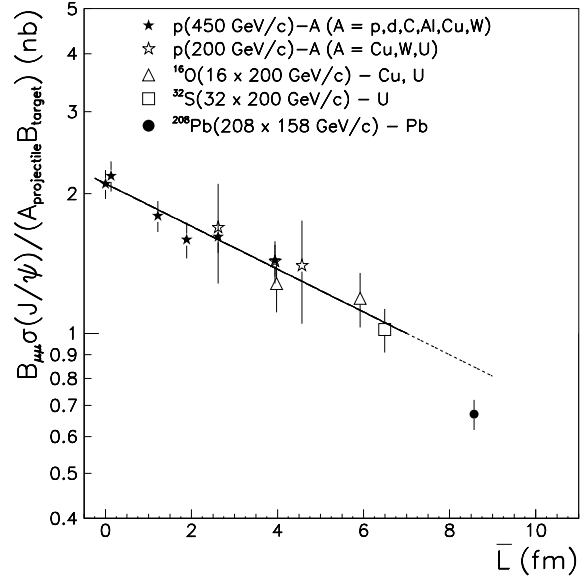
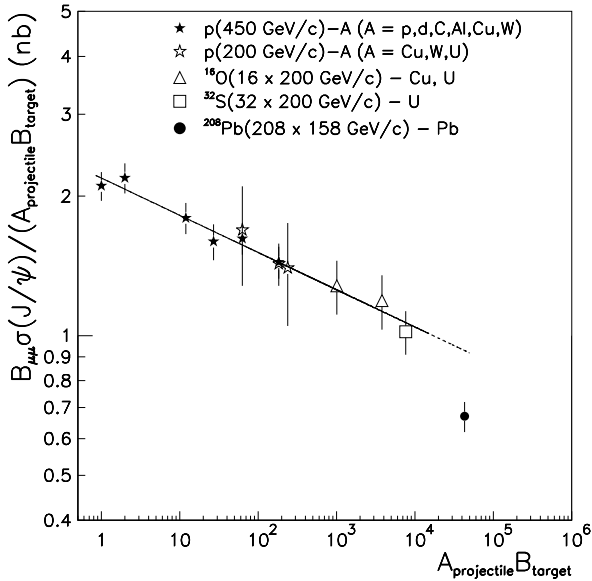


Figure 6: The J/ψ cross-section per nucleon, times b.r., with the 450 GeV results rescaled to the same kinematical domain as 200 GeV data, using the "simultaneous" fit method, (left) as a function of $A \times B$ and (right) as a function of L . The Pb-Pb result, obtained at 158 GeV, is also rescaled to 200 GeV.

S-U results, which suffer from both non negligible statistical and also systematic errors. The latter have to be taken into account when using results from different setups (NA38, NA51). Moreover, it is also based on the implicit assumption contained in the "simultaneous" fit procedure of an energy independent normal absorption cross-section, as suggested by the results available at that time.

1.4 Anomalous J/ψ Suppression in Pb-Pb Collisions

From the early first indication, it took several years to learn how to make the measurement of charmonium suppression in Pb-Pb collisions. The goal was finally reached with three different sets of p-A measurements performed from 1996 until year 2000 and two sets of Pb-Pb data collected in 1998 and 2000.

The results of the systematic set of measurements performed at CERN for 450 and 400 GeV p-A reactions do prove that at these energies, both for J/ψ and for ψ' :

- the agreement of the results with the "Glauber model parametrization" is extremely good.
- it becomes excellent when systematic uncertainties are perfectly under control. This is the case, for example, when the ratios J/ψ / Drell-Yan and ψ' / Drell-Yan are used instead of the cross-sections themselves, or when absolute cross-sections measurements become independent from incident beam flux uncertainties (which is the case for the NA50 measurements at 400 GeV).

The two points are illustrated in Figs. 7 and 8 [96,97].

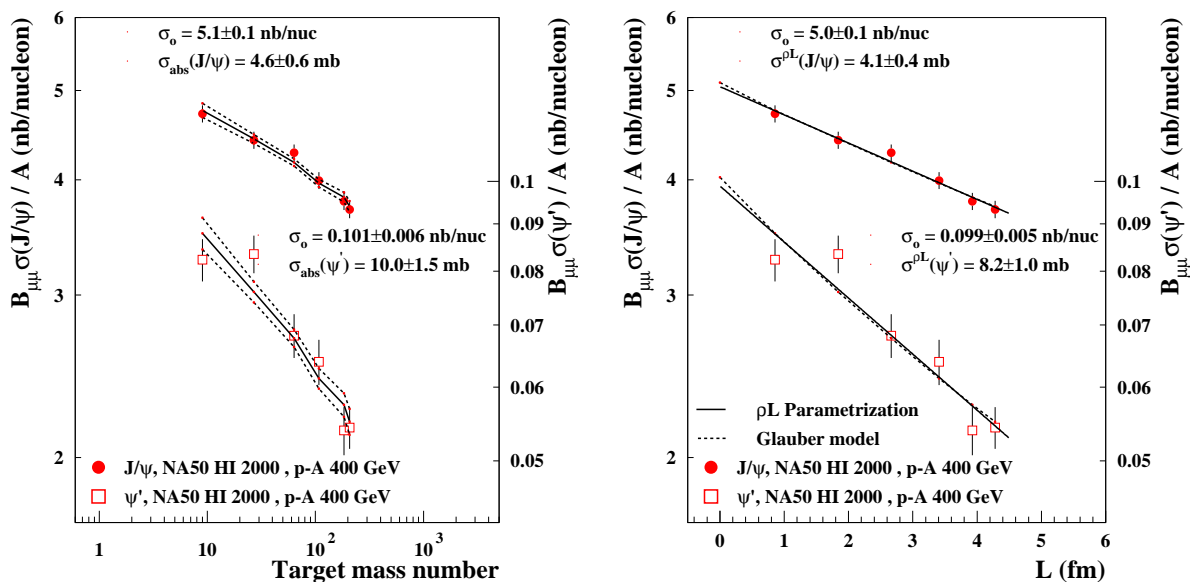


Figure 7: The J/ψ and ψ' cross-sections per nucleon adjusted by the "Glauber model" parametrization (left) and compared to the ρL parameterization (right) for the p-A data collected at 400 GeV in the rapidity range $-0.425 < y_{CM} < 0.575$. The band (left) represents the error associated to the normalization and absorption cross-section uncertainties. Within the Glauber model, the fits extrapolation to $A=1$ or to $L = \langle \rho L \rangle / \rho_0 = 0$ leads to the value of σ_0 .

1.4.1 J/ψ suppression versus the centrality of the collision

The last sample of Pb-Pb collisions data collected by experiment NA50 could benefit from the experience from previous data collections and consequent improvements of the

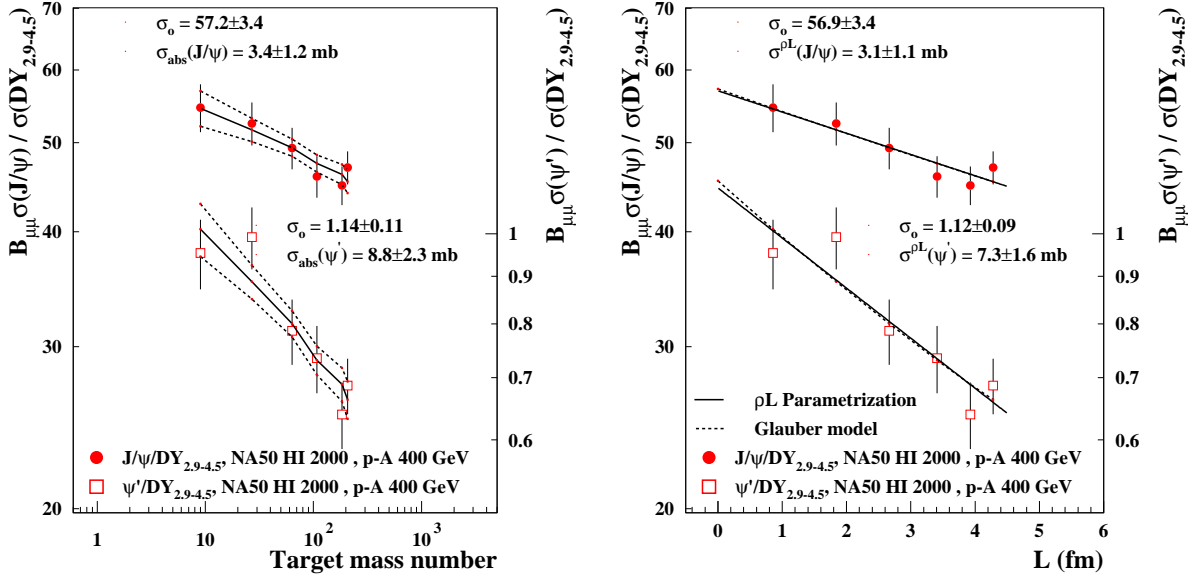


Figure 8: Same as Fig. 7 for the ratios $J/\psi / DY$ and ψ' / DY .

detector. It also benefited from overall full coherence between data and simulations, which slightly affected normalizations. All the details and results can be found in [98].

As displayed in Fig. 9, as a function of the neutral transverse energy E_T used here as the centrality estimator, the ratio of cross-sections $B_{\mu\mu} \sigma_{J/\psi} / \sigma_{DY}$ persistently decreases, from peripheral to central collisions by a factor of ~ 2.5 , showing no saturation in the decrease even for the most central collisions. The absorption pattern is here compared to the normal nuclear absorption curve as determined from the most recent and accurate p-A results obtained in the same experiment at 450 and 400 GeV together with results obtained from S-U data collected at 200 GeV. The technique of the “simultaneous” fit described in section 3.2 leads to a normal absorption cross-section $\sigma_{abs} = 4.2 \pm 0.4$ mb and provides part of the rescaling factor needed, from 450/400 GeV to 200 GeV. The advantage of using S-U results here is that it leads to minimal uncertainties in the energy rescaling factor which is “experimentally” determined, in part at least, as explained before. The curve is then further analytically rescaled to 158 GeV under the assumption that σ_{abs} is energy independent. The comparison with the normal absorption curve shows that the data behave normally for the most peripheral collisions while increasingly departing from this normal behaviour with increasing centrality.

It has been pointed out that this normal suppression reference could be biased by the use of S-U data in its determination since comoving produced hadrons, for example, could already affect J/ψ production in S-U reactions. A new determination of the reference curve has therefore been implemented as detailed hereafter. Use has been made of the most precise results on absolute J/ψ production cross-sections obtained by NA50 in p-A collisions at 450 and 400 GeV together with the results obtained at 200 GeV, again in p-A collisions exclusively, by experiments NA38 [99] and NA3 [100]. The Glauber “simultaneous fit” method detailed in section 3.2 leads then to an absorption cross-section $\sigma_{abs} = 4.1 \pm 0.4$ mb which, it is worth noting, is in excellent agreement with the value of 4.2 ± 0.4 mb obtained from the ratio of cross-sections $J/\psi / Drell\text{-}Yan$. Incidentally,

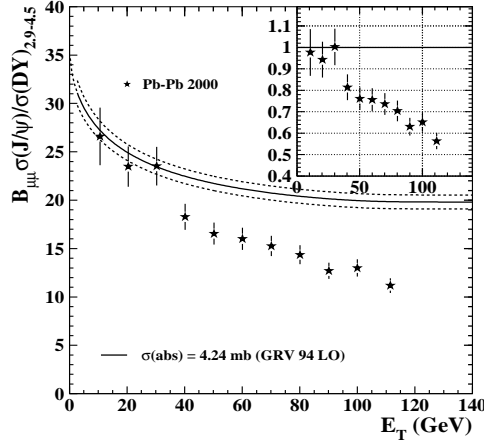


Figure 9: The ratio J/ψ / Drell-Yan compared to the normal absorption cross-section deduced from p-A and S-U measurements. The inset shows the ratio *data* / (*normal suppression*).

from the precisely measured ratio of J/ψ cross-sections in p-p and p-Pt by experiment NA3 at 200 GeV, one gets, from a completely independent determination, using the same Glauber approach, an absorption cross-section of $\sigma_{abs} = 4.1 \pm 1.0$ mb when restricted to the rapidity interval of NA50 Pb-Pb data, which, independently, strongly supports the same numerical value for σ_{abs} at 450/400 and 200 GeV incident proton energies. As detailed in [101], Figure 10 (left and center) illustrates the method and further shows that results from O-Cu, O-U and even S-U data exhibit, within errors, a so-called normal p-A like behaviour. Figure 10 (right) confirms, that with respect to a pure p-A reference curve, J/ψ is “anomalously” suppressed in Pb-Pb collisions at 158 GeV. It is worthwhile underlining here that the new reference curve for the ratio J/ψ / Drell-Yan at 158 GeV is partly deduced by analytical rescaling: the J/ψ cross-section is rescaled from 200 to 158 GeV with a Schuler-type formula [97,102] and, on the other side, the appropriate factor is applied to the Drell-Yan cross-section to rescale it from 450 to 158 GeV. This pure p-A “normal” reference curve has identical shape as the one which was also making use of S-U data. It is globally lower by a factor of 0.6% whereas its experimental uncertainty is increased by a factor 2. The most recent results obtained from Pb-Pb can now be compared with this new exclusively p-A based reference curve. As a function of three independently measured quantities tagging the centrality of the collision (see section 2), the J/ψ survival pattern exhibits very similar trends, as shown in Fig. 11.

The three independent analyses are displayed together in Fig. 12 after conversion of their originally used centrality estimator to the average number of participant nucleons in the reaction, N_{part} . The remarkable agreement between the results of the three analyses, underlines the coherence, equivalence and deep understanding of the data provided by the three independent detectors used to estimate the centrality of the collision.

It is worth recalling that E_T and the charged particle rapidity density at mid-rapidity are directly related to the energy density reached in the collision, through the Bjorken formula [109], while the forward energy measured in the ZDC is more strongly correlated

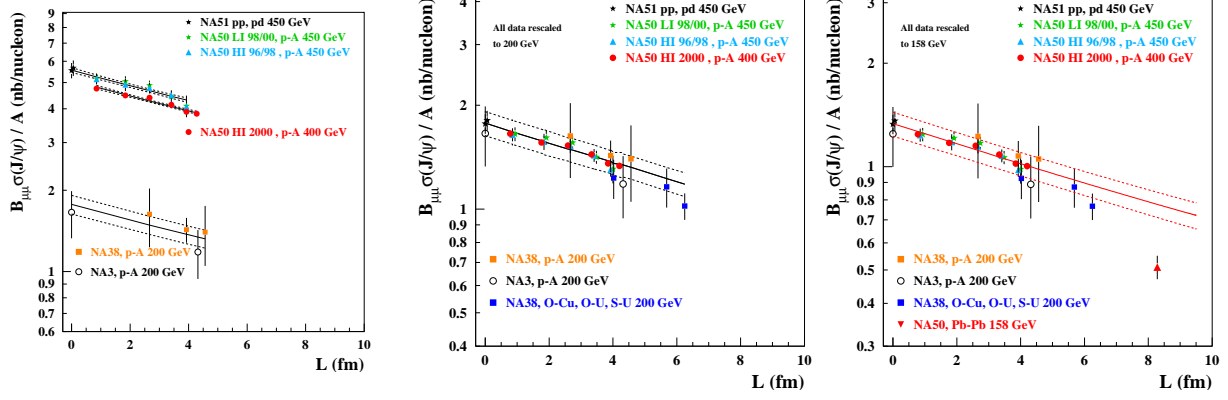


Figure 10: J/ψ cross-sections per nucleon in p-A collisions as a function of L . *Left:* Results obtained at 450, 400 and 200 GeV separately. *Center:* Same results rescaled to 200 GeV and compared with results from light nuclei collisions. *Right:* Same results rescaled to 158 GeV and further compared with J/ψ production in Pb-Pb collisions.

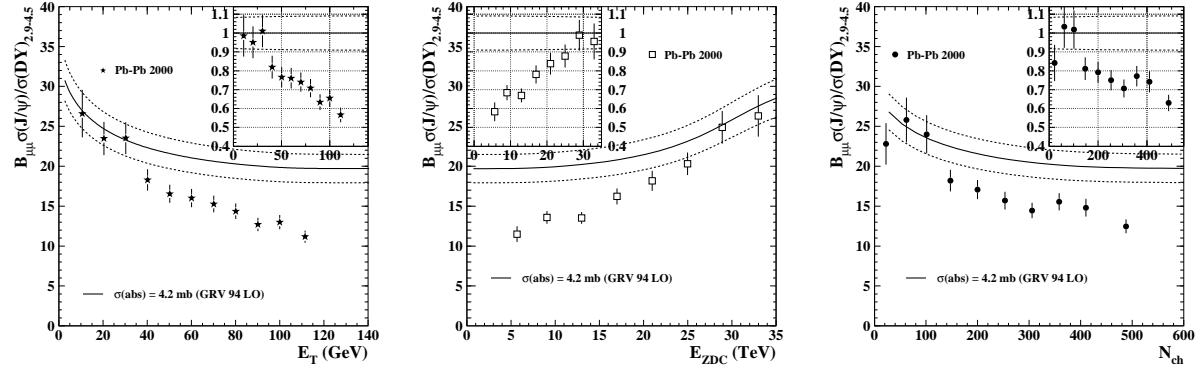


Figure 11: The ratio of cross-sections $J/\psi / \text{Drell-Yan}$ in Pb-Pb collisions as a function of, from left to right, the neutral transverse energy, the “very forward” hadronic energy and the charged multiplicity. The curve displays the normal suppression pattern as deduced from p-A interactions only. The insets show the ratio $\text{data} / (\text{normal suppression})$.

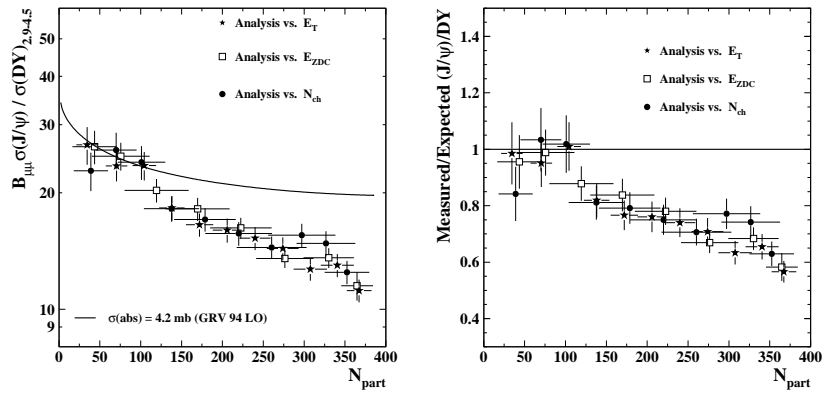


Figure 12: The $J/\psi / \text{Drell-Yan}$ cross-sections ratio as a function of N_{part} from three analysis originally using the different centrality estimators, compared to (left) and divided by (right) the normal nuclear absorption pattern.

to the geometry of the collision, and a simple robust estimator of N_{part} . Note that at SPS energies, for a given interacting system, both E_T and N_{ch} are linearly proportional to N_{part} , as expected in the framework of the wounded nucleon model, up to the most central collisions (see, for instance, Refs. [66] and [103]).

1.4.2 The transverse momentum dependence of J/ψ suppression

The p_T spectra of the surviving J/ψ 's have been studied by experiment NA50 [104] and, in particular, from their most precise sample of Pb-Pb interactions at 158 GeV collected in year 2000 [105]. The value of $\langle p_T^2 \rangle$ for the surviving J/ψ 's is plotted in Fig. 13 as a function of E_T . The overall behaviour exhibits a steady increase with centrality, from the most peripheral collisions and up to $E_T \simeq 60$ GeV. This value corresponds to $L \simeq 8.23$ fm and $\epsilon = 2.97$ GeV/fm³. The data also show that, for high centralities, no increase is seen up to the most central collisions.

In order to investigate the underlying mechanism that leads to the observed increase of $\langle p_T^2 \rangle$ for the more peripheral collisions, a comparison is made between different colliding systems as shown in Figs. 15 and 16. As a function of L , the same linear dependence is observed whatever the colliding system, with a slope apparently independent of the energy of the colliding nuclei. The first observation of this behaviour at 200 GeV based on results from NA3 [100] and NA38 [106, 107] have been successfully interpreted in terms of initial-state parton multiple scattering and analytically described by $\langle p_T^2 \rangle = \langle p_T^2 \rangle_{pp} + a_{gN} \times L$.

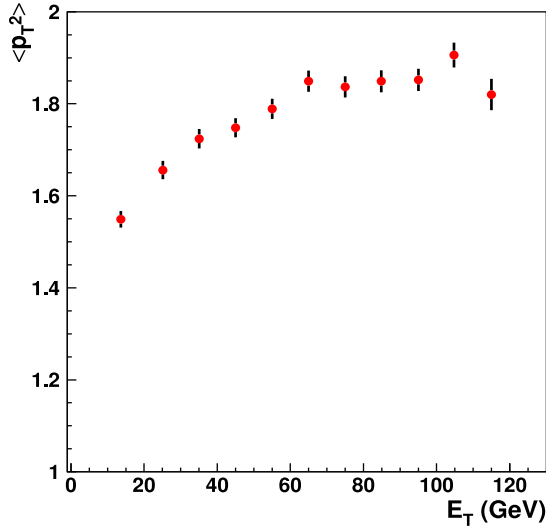


Figure 13: The average $\langle p_T^2 \rangle$ as a function of centrality, estimated from E_T , for the surviving J/ψ 's in Pb-Pb collisions at 158 GeV.

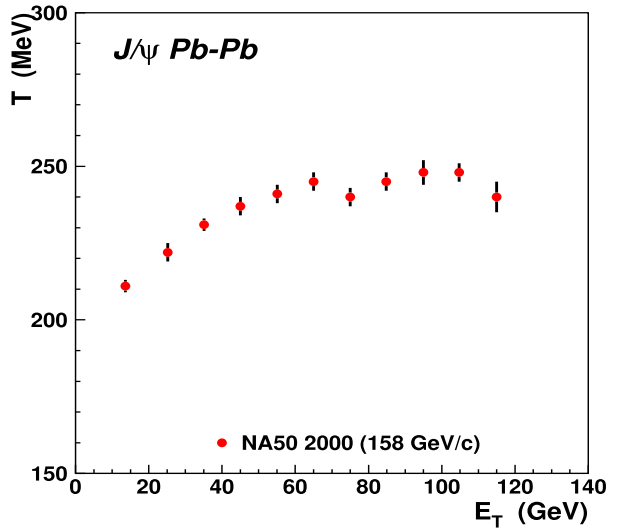


Figure 14: The transverse mass inverse slope parameter T of the surviving J/ψ 's as a function of centrality, estimated from E_T , in in Pb-Pb collisions at 158 GeV.

All the samples of J/ψ considered here are roughly in the same y_{lab} range, namely $3 < y_{\text{lab}} < 4$. The values of a_{gN} are nicely compatible for all colliding systems and energies. Using the technique of the "simultaneous fit" for the slope and leaving free the

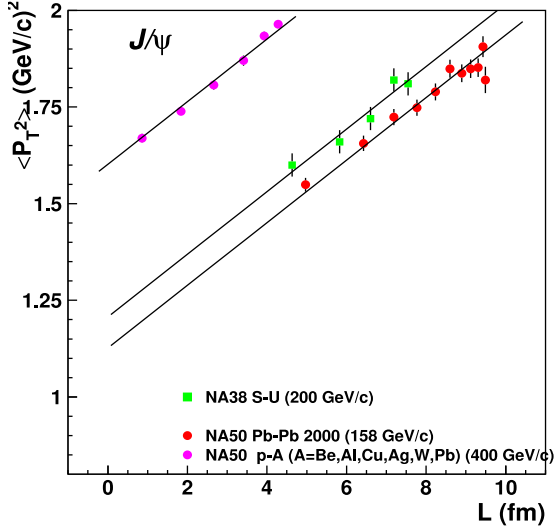


Figure 15: The average $\langle p_T^2 \rangle$ of the surviving J/ψ 's as a function of centrality, here L, for p-A (400 GeV), S-U (200 GeV) and Pb-Pb (158 GeV) with a "simultaneous" common linear fit.

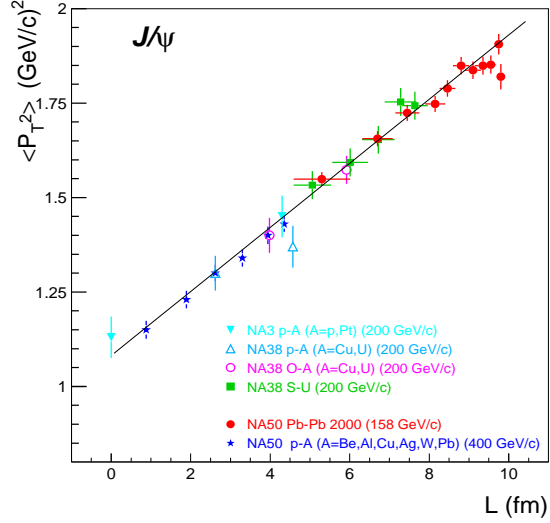


Figure 16: Same as Fig. 15, including results on p-A (200 GeV) from NA3 and NA38, O-Cu and O-U (200 GeV) from NA38. All results "experimentally" rescaled to the kinematical window used for Pb-Pb (158 GeV).

normalization factor to account for the energy change of each set of data leads to the following results:

- $\langle p_T^2 \rangle_{pp}$ increases linearly with \sqrt{s} , the total energy in the nucleon-nucleon center of mass system.
- As a function of L, the mean squared transverse momentum of the J/ψ exhibits the same increasing slope for p-A, O-Cu, O-U, S-U and peripheral Pb-Pb interactions as shown in Fig. 16, but saturates for the most central Pb-Pb collisions.
- The common fit of the increasing slope leads to $a_{gN} = 0.081 \pm 0.003$.

In an attempt to link this transverse momentum to the rate measurements, it can be empirically noticed that, as already discussed above, the measured J/ψ suppression rate has also the same, so called normal, L dependence from p-p up to S-U reactions. The specific anomalous suppression only appears for the most central Pb-Pb reactions, namely for $L > 7$ fm. This peculiar transverse momentum behaviour is also clearly seen from Fig. 14 which shows the transverse mass inverse slope parameter T , for the surviving J/ψ 's, as a function of E_T . T is deduced from a fit of the transverse mass distributions with the function $1/T \cdot M_T^2 \cdot K_1(M_T/T)$, where K_1 is the modified Bessel function. The inverse slope, T , is related to the effective temperature of the system in thermal models of particle production [107,108]. The measurements show that T increases with centrality for peripheral Pb-Pb reactions and then, slightly after anomalous suppression sets in, exhibits a trend compatible with no further increase up to the most central collisions.

The p_T dependence of J/ψ suppression has been further studied in order to investigate what are the p_T features of the suppressed J/ψ 's, as a function of the centrality of the collision. In order to be independent from any external input related to the p_T distribution

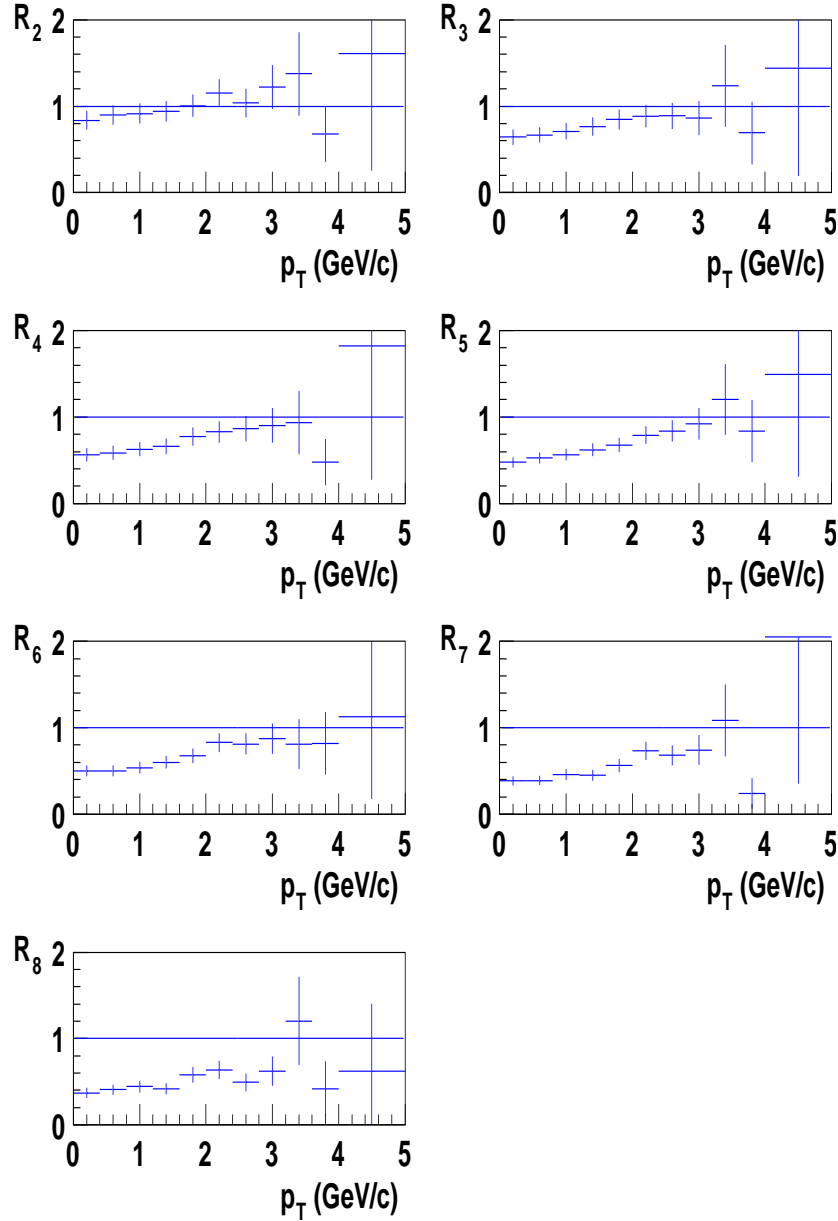


Figure 17: The ratio of the J/ψ p_T distribution in a given bin of centrality to the same distribution for the most peripheral bin. With respect to the latter, the low p_T part of the distributions depletes with increasing centrality.

of the suppressed J/ψ 's, NA50 has limited its study to the ratio of the p_T spectra obtained in various centrality bins with respect to the spectrum obtained in the most peripheral one (a procedure which will be later known as R_{CP}). For statistical reasons of this two dimensional study, J/ψ and Drell-Yan events have been considered within eight different centrality bins only. Within each centrality bin, the p_T distribution of the J/ψ has been studied, normalized to the total number of Drell-Yan events with the same centrality, i.e. to the "average number of nucleon-nucleon collisions" in the considered bin. Thus, the integral of the p_T spectrum in each of the bins is the ratio J/ψ / Drell-Yan, as would be

plotted, for example, in Fig. 9 dividing the whole centrality range in only 8 bins (instead of 11). The ratios F_i and R_i are thus defined as:

$$F_i = \frac{dN_{J/\psi}^i/dp_T}{N_{DY(M>4.2 \text{ GeV}/c^2)}^i} \quad \text{and} \quad R_i = \frac{F_i}{F_1}$$

where i is the i^{th} centrality bin, $dN_{J/\psi}^i/dp_T$ is the number of J/ψ events of a given p_T in centrality bin i and $N_{DY(M>4.2 \text{ GeV}/c^2)}^i$ is the *total* number of Drell-Yan events with $M > 4.2 \text{ GeV}/c^2$ in centrality bin i .

Figure 17 displays the p_T dependence of the seven ratios R_i . It shows that with increasing centrality, the lower the p_T the higher the suppression. Moreover and within statistical uncertainties, it suggests that, for transverse momenta larger than $2.5 \text{ GeV}/c$, the shape of the p_T spectrum of J/ψ is independent of centrality and very close to the one observed in the most peripheral collisions. It should be underlined here that, as all R_{CP} studies, this approach does not allow to easily disentangle between transverse momentum spectrum modifications due to normal and to abnormal suppression separately. As an illustration, a similar study made for S-U reactions which are only subject to normal J/ψ suppression exhibits nevertheless qualitatively similar features [107].

1.4.3 J/ψ survival pattern: from p-p to Pb-Pb

Figure 18 shows the ratio of cross-sections J/ψ / Drell-Yan for the collision systems studied up to now, from the lightest p-p up to the heaviest Pb-Pb [98]. When necessary, they have been reanalyzed in order to ensure a fully coherent data selection and treatment. They have also been rescaled to an incident beam momentum of $158 \text{ GeV}/c$ when required. This rescaling, both for energy and rapidity coverage, has used the ‘‘simultaneous fit’’

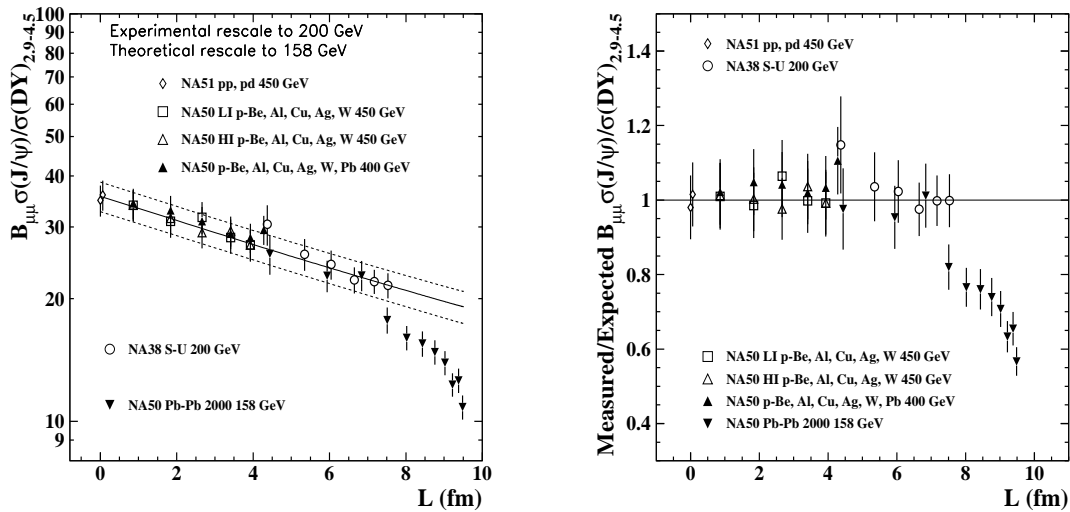


Figure 18: The J/ψ / Drell-Yan ratio of cross-sections vs. L , for several collision systems, compared to (left) and divided by (right) the normal nuclear absorption pattern. All data are rescaled to $158 \text{ GeV}/\text{nucleon}$.

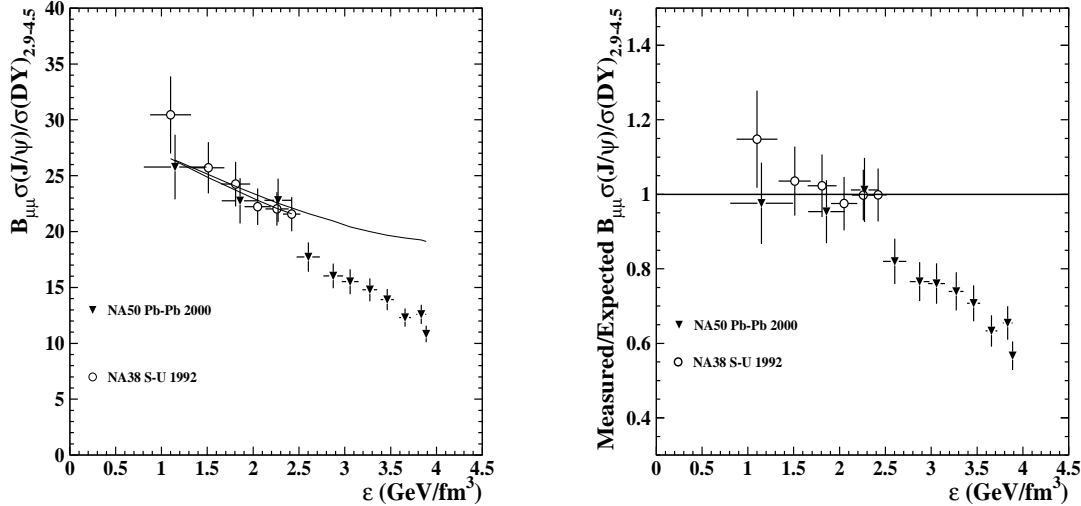


Figure 19: Same as Fig.18 for S-U and Pb-Pb collisions only, as a function of energy density. The absorption curves for S-U and Pb-Pb in the *left* panel of the figure are slightly different because the relation between energy density and L (obtained from a Glauber calculation) depends on the colliding nuclei.

method to bring the results obtained at higher momenta down to 200 GeV/ c and an analytical calculation to further bring the 200 GeV results down to 158 GeV. Figure 19 shows the same ratio of cross-sections J/ψ / Drell-Yan obtained in S-U and in Pb-Pb collisions as a function of ϵ , the energy density averaged over the whole transverse area of the collision. The latter is obtained with the Bjorken [109] formula from the total transverse energy deduced from the measurement of its neutral component in the electromagnetic calorimeter [113]. It shows that the departure from the normal nuclear absorption curve sets in for energy densities around 2.5 GeV/fm³, just above the values reached in the most central S-U collisions.

The numerical values of the different variables used as centrality estimators are given in Table 1 for the Et bins chosen above for Pb-Pb collisions at 158 GeV. They have been calculated with the Glauber model and assuming an initial formation time $\tau_0 = 1$ fm/ c . The values for S-U collisions at 200 GeV are given in Table 2. They include, in the errors, the resolution of the electromagnetic calorimeter. The authors [113] consider that the relative scale between S-U and Pb-Pb is robust, while the absolute values could be affected by a 20%-25% systematic uncertainty.

2 Features of ψ' Suppression at SPS Energies

As known since long, ψ' production is also affected by nuclear effects in p-A collisions. This is now quantitatively supported with precise results from NA50 based on two different samples of data collected at 450 and 400 GeV with incident protons on Be, Al, Cu, Ag, W and Pb targets [96,97,110,111]. The results, obtained with a Glauber parametrization

Bin	E_T (GeV)		N_{part}		b (fm)		L (fm)		ϵ (GeV/fm ³)	
	range	average	average	rms	average	rms	average	rms	average	rms
1	3–15	10.6	34	13	11.8	0.7	4.44	0.72	1.15	0.34
2	15–25	20.4	70	13	10.3	0.5	5.94	0.42	1.86	0.20
3	25–35	30.3	104	14	9.2	0.4	6.84	0.33	2.27	0.15
4	35–45	40.2	138	16	8.2	0.4	7.51	0.27	2.60	0.13
5	45–55	50.2	172	17	7.3	0.4	8.02	0.23	2.87	0.11
6	55–65	60.1	206	18	6.5	0.4	8.43	0.20	3.06	0.09
7	65–75	70.1	240	19	5.6	0.5	8.76	0.17	3.27	0.08
8	75–85	80.1	274	20	4.8	0.5	9.02	0.15	3.46	0.07
9	85–95	90.1	308	21	3.9	0.6	9.22	0.12	3.66	0.06
10	95–105	100.0	341	20	2.8	0.7	9.38	0.11	3.83	0.05
11	105–150	111.5	367	15	1.7	0.7	9.48	0.06	3.89	0.04

Table 1: Centrality classes for Pb-Pb interactions at 158 GeV based on the transverse energy measurement. For each class are listed the E_T range and weighted average, together with the average and rms values of N_{part} , b , L and ϵ .

Bin	E_T (GeV)		N_{part}		L (fm)		ϵ (GeV/fm ³)	
	range	average	average	rms	average	rms	average	rms
1	13–28	22.1	31.3	9.1	4.37	0.54	1.04	0.22
2	28–40	34.3	50.0	9.7	5.35	0.43	1.46	0.18
3	40–52	46.3	66.7	10.8	6.04	0.41	1.76	0.16
4	52–64	58.3	83.5	11.7	6.65	0.41	2.01	0.15
5	64–76	70.2	98.8	11.0	7.17	0.38	2.22	0.13
6	76–88	81.7	109.0	8.2	7.53	0.29	2.38	0.09

Table 2: Same as previous table, for S-U collisions at 200 GeV.

separately at 450 and 400 GeV, are quite compatible. Their combination leads to an absorption cross-section of 8.3 ± 0.9 mb from the values of production cross-sections per nucleon and 7.7 ± 0.9 mb from the ratios $\psi' / \text{Drell-Yan}$, with minimal systematic uncertainties in this case [96]. These values can be compared to 4.18 ± 0.35 mb as obtained for J/ψ .

The ψ' study [112] made with Pb-Pb interactions at 158 GeV is based on only 1285 ψ' events. It shows that both with respect to Drell-Yan, and also with respect to the J/ψ , ψ' production decreases with increasing centrality, as displayed in Figs. 20 and 21. It is worthwhile noting here that the Drell-Yan mass range chosen here to normalize the

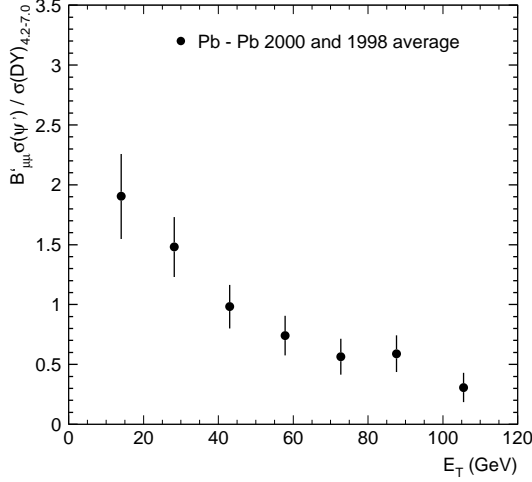


Figure 20: The ratio of cross-sections $B'_{\mu\mu}\sigma(\psi')/\sigma(DY)$ as a function of E_T , with DY in the mass range 4.2-7.0 GeV/c².

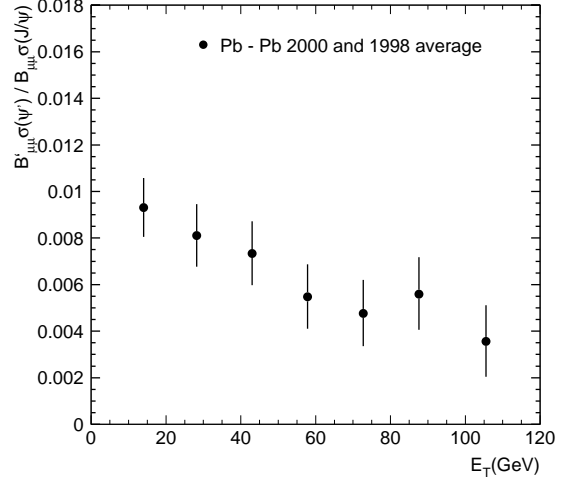


Figure 21: The ratio $B'_{\mu\mu}\sigma(\psi')/B_{\mu\mu}\sigma(J/\psi)$ as a function of E_T .

ψ' yield is 4.2–7.0 GeV/c². Scaling up the results to the mass range used in the J/ψ suppression studies, namely 2.9–4.5 GeV/c², requires to apply the factor 7.96, which is the ratio between the Drell-Yan cross-sections in the two mass domains. In order to investigate whether ψ' production exhibits any abnormal suppression pattern in nucleus-nucleus collisions, the production cross-sections per nucleon-nucleon collision (or, equivalently, normalized to Drell-Yan) are compared, after appropriate rescaling to the same kinematical domain, between p-A, SU and Pb-Pb collisions [96, 97].

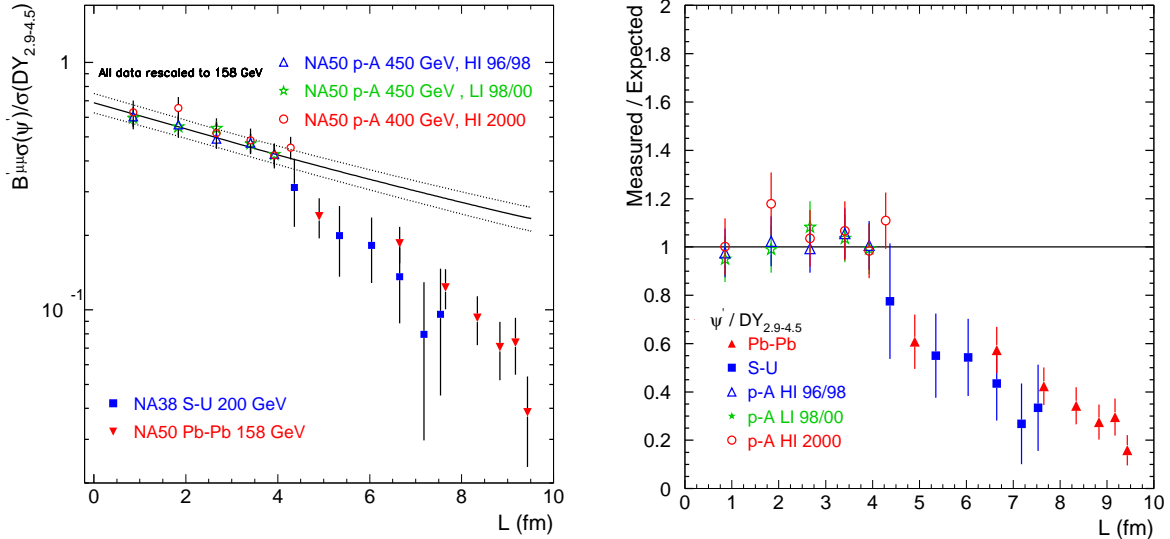


Figure 22: The ψ' / Drell-Yan ratio of cross-sections vs. L , for several collision systems, compared to (left) and divided by (right) the normal nuclear absorption pattern. All data are rescaled to 158 GeV/nucleon.

The left panel of Fig. 22 shows the ratio $B'_{\mu\mu}\sigma(\psi')/\sigma(DY)$ as a function of L . The measured

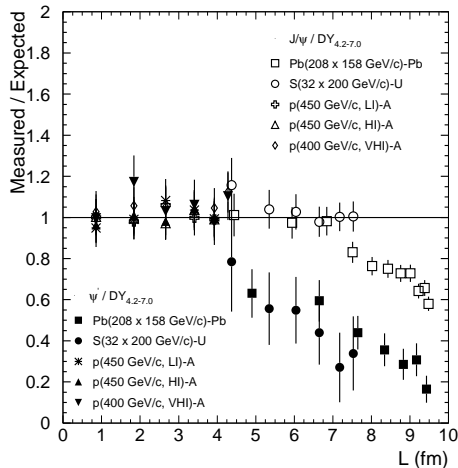


Figure 23: Same as Fig. 22 (right) for J/ψ and ψ' on same L scale.

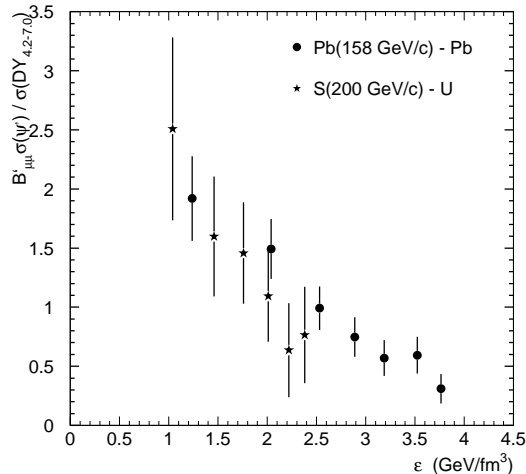


Figure 24: The ratio $B'_{\mu\mu}\sigma(\psi')/\sigma(\text{DY})$ as function of the energy density.

suppression patterns suggest the following features:

- A fair agreement with exponential behaviours, with two different regimes, one for proton and a different one for ion-induced reactions.
- A similar centrality dependence for S-U and Pb-Pb interactions.

Using the approximate exponential parametrization to describe ψ' absorption as a function of L, the fit of the data leads to an absorption cross-section of 7.3 ± 1.6 mb in p-A collisions, while a much higher value, 19.2 ± 2.4 mb, is obtained for ion-ion collisions (S-U and Pb-Pb fitted simultaneously). The right panel of Fig. 22 shows, as a function of L, the ratios between the measured ψ' yields, normalized to Drell-Yan, and the corresponding expected “normal nuclear absorptions”, as extrapolated from p-A measurements. The difference between the suppression patterns for J/ψ and ψ' is shown in Fig. 23. The ψ' suppression for S-U and Pb-Pb collisions is shown in Fig. 24 as a function of the energy density which is calculated as described in detail in [113]. The numerical values of L, N_{part} and the energy density ϵ used for the ψ' studies in Pb-Pb collisions are given in Table 3.

3 More Results from SPS and RHIC

After the systematic studies carried out by experiments NA38, NA50 and NA51, two other experiments were aimed at extending the knowledge on charmonium suppression in ultrarelativistic heavy ion interactions.

At the CERN-SPS, in a fixed target experiment, the NA60 collaboration uses basically the same muon spectrometer as NA50 [88] except for the centrality estimate which is based exclusively on the very forward calorimeter measurements. The NA50 detector is upgraded with a silicon pixel telescope, located in the target region, which leads to an extremely precise determination of the origin of the measured tracks and, consequently, to a better dimuon mass resolution. Data have been collected to study In-In collisions

Bin	E_T (GeV)		N_{part}		L (fm)		ϵ (GeV/fm ³)	
	range	average	average	rms	average	rms	average	rms
1	3–20	13.9	44.6	17.7	4.90	0.84	1.24	0.37
2	20–35	28.2	96.7	18.0	6.65	0.44	2.04	0.20
3	35–50	43.0	147.1	19.3	7.65	0.31	2.53	0.14
4	50–65	57.8	197.7	20.6	8.34	0.24	2.89	0.11
5	65–80	72.7	248.6	22.0	8.83	0.18	3.19	0.09
6	80–95	87.6	299.2	23.0	9.17	0.14	3.52	0.07
7	95–150	105.9	353.3	22.4	9.43	0.10	3.76	0.06

Table 3: Mean free path crossed by the $c\bar{c}$ pair inside the nucleus, number of participating nucleons and energy densities for each Pb-Pb E_T range.

with an incident In beam of 158 GeV/c [114] and also p-A reactions with incident proton beams of both 400 and 158 GeV/c.

At the RHIC collider at BNL, the PHENIX experiment studies p-p [115,116], d-Au [117, 118], Cu-Cu [119] and Au-Au [120,121] collisions at much higher energies, namely 200 GeV in the c.m.s. and, consequently, at higher energy densities than those reached at the CERN-SPS. It makes use of a detector specifically designed to study heavy ion collisions at RHIC [122].

Some of the results obtained by these experiments in their studies of J/ψ suppression are summarized hereafter.

3.1 J/ψ Suppression in In-In Collisions at 158 GeV

In a first analysis strategy, experiment NA60 follows the approach adopted by experiments NA38/NA50 and makes use of the ratio $J/\psi / \text{Drell-Yan}$. This ratio is free from systematic uncertainties and provides its own absolute normalization, without any external input. It thus leads to the most robust estimate of the J/ψ yield normalized to the number of nucleon-nucleon collisions, through the experimentally measured Drell-Yan events. Unfortunately the number of Drell-Yan events in NA60 is extremely small and allows, in a centrality dependent study, for only 3 bins in centrality. In order to identify any anomalous behavior, the results are compared with normal nuclear absorption as determined experimentally by experiments NA38/NA50. The results can then be expressed in terms of the ratio "measured/expected", where "expected" refers to normal nuclear absorption corresponding to an absorption cross-section of 4.18 ± 0.35 mb. The 3 measured ratios are plotted in Fig. 25 as a function of N_{part} .

In a second approach, the measured "unnormalized" J/ψ yield is directly compared to the analytically calculated centrality distribution of J/ψ . The latter is derived in the frame of the Glauber model using the same absorption cross-section of 4.18 mb. Relative normalization between the data and the reference curve is obtained by requiring that the ratio of the centrality integrated distributions is equal to the centrality integrated ratio

J/ψ / Drell-Yan. Fig. 26 shows both the measured and calculated distributions as a function of centrality, estimated here from the forward energy of the spectators nuclei. Their ratio is plotted in Fig. 25 as a function of N_{part} .

The method does not suffer any more from the limited number of Drell-Yan events, makes use of the statistical power of the J/ψ sample and reaches unprecedented small statistical uncertainties. It should be noted here, nevertheless, that the same method could have been applied by experiment NA50 which, indeed and as compared to NA60, had more than a factor 3 larger J/ψ sample of events. The NA50 experiment made the choice of studying the J/ψ suppression pattern in Pb-Pb collisions through the robust, unbiased J/ψ / Drell-Yan ratio which is free, at first order, from all potential systematic experimental effects which cancel out in the ratio. It is also free from analytical model dependent descriptions of the detectors. It therefore minimizes systematic uncertainties, sometimes difficult to find and evaluate. NA50 discarded this type of analysis from its final results which are thus dominated, by far, by pure statistical uncertainties in the Drell-Yan sample of events.

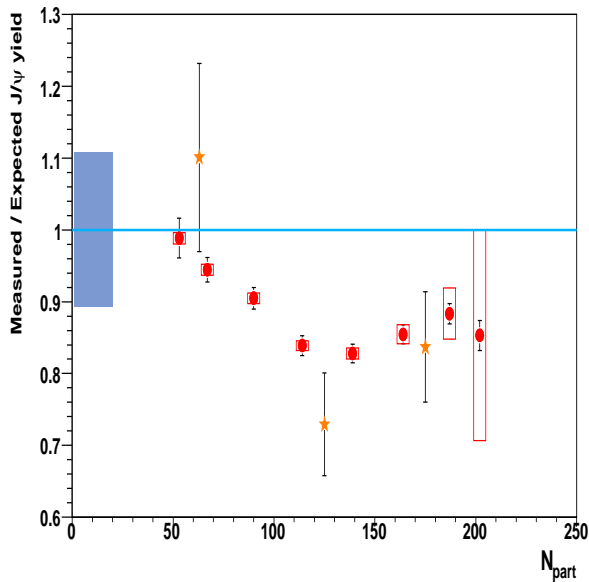


Figure 25: Centrality dependence of the J/ψ suppression in In-In collisions for the ratio $\sigma_{J/\psi}/\sigma_{\text{DY}}$ (star symbols) and for the J/ψ absolute yield (circle symbols). Also shown are the common global systematic error (left box) and the relative point to point uncertainties.

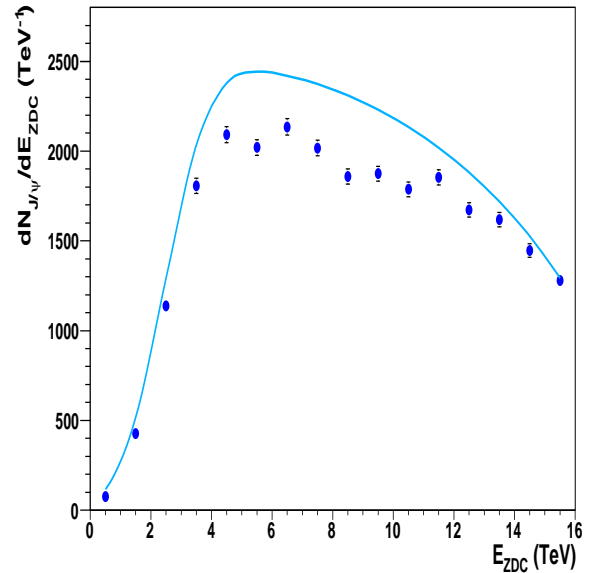


Figure 26: The J/ψ E_{ZDC} distribution (circles), compared with expectations from nuclear absorption (line).

The results of experiment NA60 can be compared to those of NA50 shown in Fig. 12 which superposes the results obtained, separately, through the three independent centrality estimators. The suppression patterns in Pb-Pb and In-In are qualitatively similar and compatible, thanks to the errors quoted by NA50. In some more detail, nevertheless, some differences can be noticed in this comparison.

The results on In-In do not exhibit a solid evidence of normal behaviour for peripheral collisions. There is one single centrality point with a ratio "measured/expected" amount-

ing to 0.99 ± 0.06 , which is somewhat insufficient to support a constant trend close to unity in the vicinity of $N_{\text{part}} \simeq 50$. On the other hand, the Pb-Pb results do exhibit a normal behaviour extending over 2 or 3 centrality bins and up to about $76 N_{\text{part}}$. Taking into account the resolution of the centrality measurement, In-In collisions would depart from normal behaviour for $N_{\text{part}} \simeq 80 N_{\text{part}}$ corresponding to an energy density of $1.5 \text{ GeV}/\text{fm}^3$. For Pb-Pb collisions, the departure is detected at $N_{\text{part}} \simeq 100 N_{\text{part}}$ when using the same centrality detector and at $N_{\text{part}} \simeq 120 N_{\text{part}}$ when using the most precise centrality estimator, which corresponds to 2.25 and $2.45 \text{ GeV}/\text{fm}^3$ respectively.

The In-In and Pb-Pb suppression patterns themselves show different trends. Pb-Pb exhibits a steady decreasing trend, in particular for $N_{\text{part}} > 150$, as opposed to a kind of an unexpected rise, starting for $N_{\text{part}} > 140$, in the case of In-In. This rise could perhaps accommodate, within errors, some flat behaviour.

3.2 J/ψ Suppression in A-A Collisions at $\sqrt{s} = 200 \text{ GeV}$

The PHENIX experiment at RHIC measures J/ψ production at $\sqrt{s} = 200 \text{ GeV}$, for rapidities $|y| < [1.2, 2.2]$ and also $|y| < 0.35$. The study is made in terms of the "nuclear modification factor", R_{AB} , defined as:

$$R_{\text{AB}}(y) = \frac{(d\sigma/dy)_{\text{A-B}}}{N_{\text{coll}} (d\sigma/dy)_{\text{p-p}}}$$

when referring, for example, to the reaction of nucleus A with nucleus B.

Fig. 27 shows the ratio R_{AA} for J/ψ 's of low rapidity in the collision c.m.s. obtained by the PHENIX experiment for Au-Au and Cu-Cu collisions. The same plot shows the results obtained with other colliding systems at lower energies, derived from the measurements performed at CERN. The ratio R_{AA} (or R_{AB}) is plotted as a function of the N_{part} value corresponding to the selected centrality bins made in the different analyses. It exhibits, within errors, an in-discriminable pattern for all the colliding systems, including S-U and Pb-Pb. On the other hand and from different type of studies, as detailed above, it is known that S-U behaves normally as well as the 2 more peripheral points of Pb-Pb which are plotted in the figure, whereas abnormality sets in for $N_{\text{part}} > 100$ in the case of Pb-Pb, at least. It therefore appears that this kind of representation, namely R_{AA} as a function of N_{part} , is not the most sensitive in order to experimentally detect, without external theoretical inputs, any abnormal J/ψ suppression.

Fig. 28 shows that the nuclear modification factor is a function of the J/ψ rapidity for Au-Au collisions. Indeed, this feature was already visible in fixed target p-A experiments with 200 and $800 \text{ GeV}/c$ incident protons by experiments NA3 [100] and E866 [124]. The understanding of such an observation on Au-Au at 200 GeV requires again complete experimental knowledge of the reference for the two different kinematic windows, under conditions excluding the formation of a new state of matter (see section "Discussion" below).

The J/ψ suppression has also been studied by PHENIX as a function of the transverse

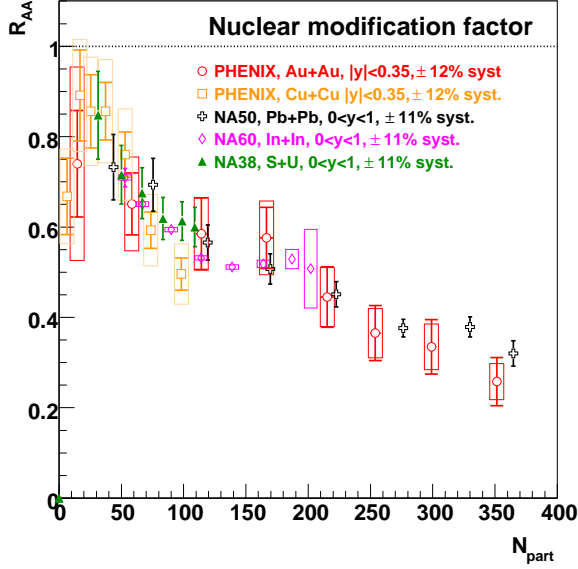


Figure 27: J/ψ nuclear modification factors for Au-Au, Pb-Pb, In-In and S-U colliding systems at their respective energies (200, 19 and 17.3 GeV) as a function of the number of participants, N_{part} .

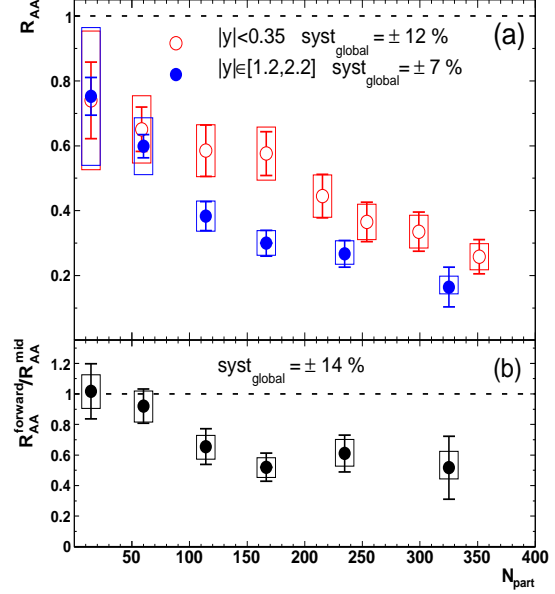


Figure 28: (a) The J/ψ nuclear modification factor for Au-Au as a function of N_{part} , for central and forward rapidities. (b) Ratio of forward/mid rapidity J/ψ R_{AA} vs. N_{part} .

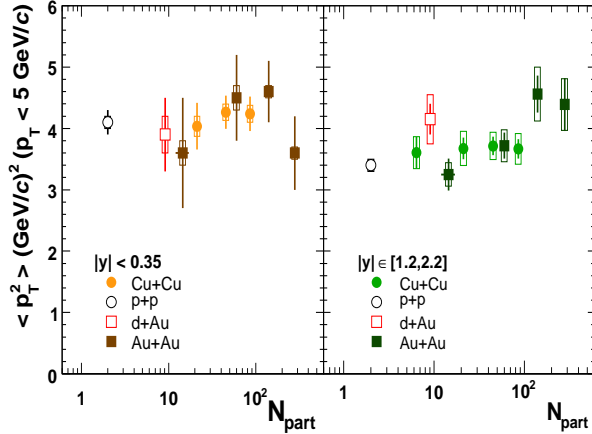


Figure 29: The surviving J/ψ average $\langle p_T^2 \rangle$ as a function of N_{part} for Au-Au, as measured by PHENIX at mid (left) and forward (right) rapidity.

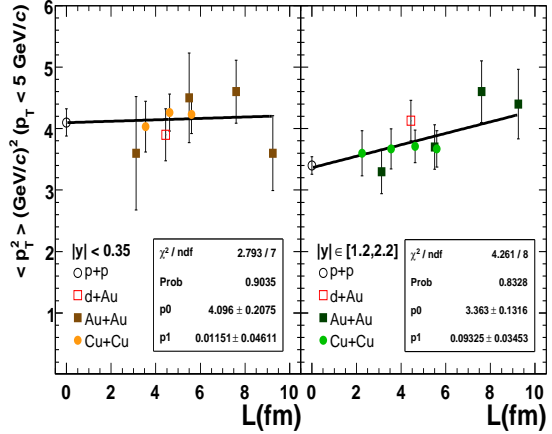


Figure 30: Same as fig. 29, as a function of L .

momentum. Fig. 29 shows, as a function of N_{part} , the values of $\langle p_T^2 \rangle$ for various colliding systems [119]. Fig. 30 [123] uses instead the variable L in order to allow a comparison with the results obtained at the SPS, successfully parametrized as a function of the path traversed by the J/ψ in nuclear matter (see Figs. 15 and 16). The PHENIX measurements are affected by very large uncertainties. Within their limited accuracy, they also

suggest a linear behaviour as a function of L , the same for all the systems which are taken here at same colliding energy. The numerical values of the corresponding fitted slopes, namely 0.012 ± 0.046 and 0.093 ± 0.035 for central and forward rapidity respectively can be compared with the accurate value measured at the SPS by the NA38/NA51/NA50 experiments which amounts to 0.081 ± 0.003 in significantly different kinematical conditions. Much more accurate measurements are obviously needed at RHIC in order to become a quantitative probe for the simplistic interpretation of the lower energy results.

4 Discussion and Evaluation

Future experimental progress could consolidate what appears already today like well established experimental evidences. The results detailed above do raise, nevertheless, two important points which are discussed hereafter.

- Anomalous J/ψ suppression in Pb-Pb collisions at $\sqrt{s} = 17.2$ GeV.
The anomalous character of the observed J/ψ suppression is the first point to be clarified if charmonium suppression is the signature of some new physics specific to high energy nucleus-nucleus collisions. For the moment, an evidence for this abnormal behaviour has been deduced from the systematic studies carried at the SPS by experiments NA38/51/50. In order to define the reference curve attached to "normality", the experiments have made use of a set of systematic measurements made on p-induced reactions at 450, 400 and 200 GeV/c. It has been found that also J/ψ 's produced in O-Cu, O-U and S-U collisions at 200 GeV behave normally, i.e. like in p-A reactions, *for the same rapidity range in the lab (or rather target) reference system*. It is with respect to this experimental reference, appropriately rescaled to 158 GeV under the explicit assumption that nuclear absorption of J/ψ is beam-energy independent from 450 down to 158 GeV, that the abnormal character of J/ψ suppression has been established for mid-central and central Pb-Pb reactions. The validity of this crucial assumption is supported by two independent fixed target experiments.

1. Experiment E866

At Fermilab, experiment E866 [124] has provided cross-section ratios measurements on p-Be and p-W at 800 GeV/c ($\sqrt{s} = 39$ GeV). The measured ratio of cross-sections remains constant within the range $-0.10 < x_f < 0.25$ or, equivalently $3.13 < y_{\text{lab}} < 4.95$. When parametrized with the Glauber model, it leads to an absorption cross-section of 2.83 ± 0.77 . This numerical value is therefore rapidity independent within the explored y_{lab} range which largely overlaps with the range $3.0 < y_{\text{lab}} < 4.0$ explored by the NA38/NA51/NA50 experiments. The latter find 4.18 ± 0.35 mb, show that nuclear absorption indeed accounts for the measurements and, furthermore, that the absorption cross-section is rapidity independent within the covered range [110,111].

2. Experiment NA3

The most precise result on the topic is found in CERN experiment NA3 [100, 125]. Their data lead to a precise value of the ratio of J/ψ production cross-sections measured directly in p-p and in p-Pt collisions in a single simultaneous

beam exposure at 200 GeV or $\sqrt{s} = 19.4$ GeV. The Glauber model description allows to derive the nuclear absorption cross-section, with appropriate treatment of errors, in the y_{lab} rapidity range where NA3 shows it stays constant, namely $3.0 < y_{\text{lab}} < 4.0$. The resulting numerical value is 4.1 ± 1.0 mb. This value is surprisingly close to the NA50 determination at 400/450 GeV, namely 4.18 ± 0.35 mb. The results obtained for p-a reactions at 800, 450/400 and 200 GeV/c suggest that the J/ψ absorption cross-section has no or little dependence on \sqrt{s} within this E_{beam} range, when considered in the same y_{lab} rapidity interval in which it stays constant. They thus support the assumption made by NA50 when rescaling the normal absorption reference curve down to 158 GeV.

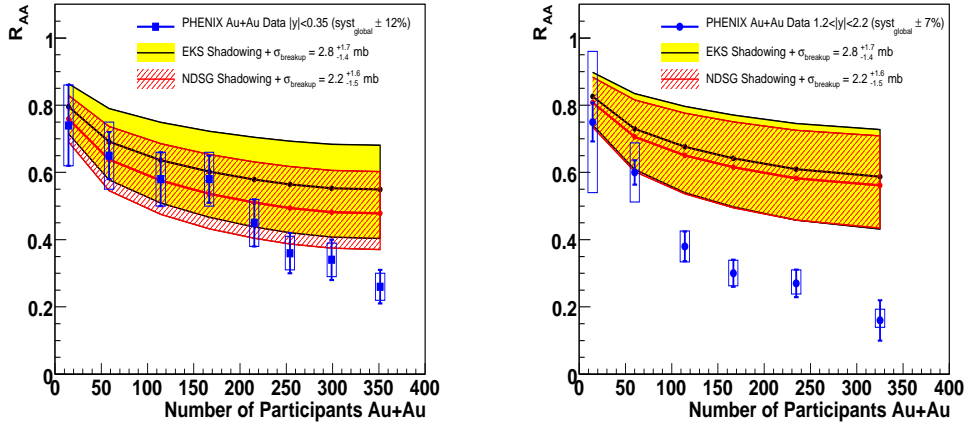


Figure 31: R_{AA} for Au-Au collisions compared to a band of theoretical curves for the σ_{abs} values found to be consistent with the d-Au data. EKS and NDSG shadowing are included for midrapidity (left). Same for forward rapidity (right).

- Is there anomalous J/ψ suppression in Au-Au collisions at RHIC ?
 In order to be able to detect an abnormal J/ψ suppression from an experimental point of view and with minimal external input, appropriate experimental references are mandatory, measured under conditions such that no new physics can reasonably be expected. The PHENIX experiment has made use of the presently available d-Au data to establish the normal suppression or "cold nuclear matter effects" pattern expected for the Au-Au measurements at RHIC [126]. Figs. 31 and 32 show the values of R_{AA} as a function of centrality as measured in Au-Au collisions compared to the pattern extracted from d-Au measurements, taking also into account the shadowing effects expected at RHIC. PHENIX conclusion is that "Neither the predictions of cold nuclear effects in heavy ion collisions based on fitting of the d-Au data with theoretical curves nor those obtained directly from the d-Au data points are well enough constrained to permit quantitative conclusions about additional hot nuclear matter effects". Much more precise reference data on d-Au collisions are needed to reach a solid conclusion.

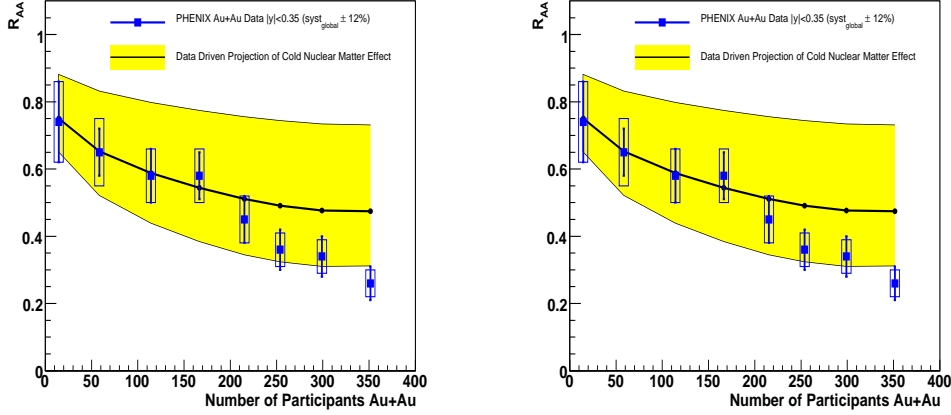


Figure 32: R_{AA} for Au-Au collisions compared to predictions of the data driven method constrained by the R_{d-Au} as a function of collision centrality, for midrapidity (left) and forward rapidity (right).

5 Summary of the Experimental Status

At the eve of the start of a new generation of experiments aimed at further studies of quarkonium abnormal suppression as a signature of QGP formation, the present experimental situation is summarized hereafter.

1. The production of J/ψ suffers from cold matter nuclear effects also called normal nuclear absorption. This absorption can be interpreted as resulting from interactions of a given $c\bar{c}$ state while propagating in normal cold nuclear matter. Quantitatively, the corresponding absorption cross-section has been precisely measured in p-A interactions up to p-Pb, at $\sqrt{s} = 29.0$ and 27.4 GeV. For a J/ψ with rapidity in the range $3.0 < y_{lab} < 4.0$. with respect to the traversed nuclear matter, the best determination of the absorption cross-section leads to $\sigma_{abs}^{J/\psi} = 4.2 \pm 0.35$ mb. The values derived from data collected at $\sqrt{s} = 39$ and 19.3 GeV in the same rapidity range are in in very good agreement with this devoted measurement. Measurements performed on light nuclei interactions, namely O-S, O-U and S-U at 19.3 GeV show excellent compatibility with the above quoted cross-section and, therefore, J/ψ production in such reactions only suffers from normal nuclear effects. There is thus compelling evidence that the value of σ_{abs} in the same rapidity window stays the same for $\sqrt{s} = 17.3$
2. The production of ψ' also suffers from cold matter nuclear effects. Systematic measurements performed on p-A reactions at 29.0 and 27.4 GeV lead to a cross-section $\sigma_{abs}^{\psi'} = 7.7 \pm 0.9$ mb, significantly higher than $\sigma_{abs}^{J/\psi}$.
3. From comparison with appropriate references deduced from the measurements on p and light ion-induced collisions, J/ψ production in Pb-Pb interactions at 17.3 GeV exhibits only normal nuclear effects up to an energy density of $\epsilon = 2.5$ GeV/fm³. An abnormal absorption appears above this value of ϵ and significantly increases

with increasing energy density, up to an abnormal suppression factor of 0.6, for the most central Pb-Pb collisions.

4. In contrast with the J/ψ patterns, ψ' production exhibits an abnormal suppression starting with S-U reactions at 19 GeV. The observed suppression pattern is in very good agreement with the one exhibited by Pb-Pb interactions at 17.3 GeV. They both lead to an absorption cross-section of $\sigma_{\text{abs}}^{\psi'} = 19.2 \pm 2.4 \text{mb}$ as compared to 7.3 ± 1.6 for normal ψ' absorption. Abnormal suppression for ψ' starts above an energy density $\epsilon = 1 \text{ GeV}/\text{fm}^3$.
5. Data obtained from In-In collisions at 17.3 GeV tend to qualitatively support the suppression pattern measured in Pb-Pb collisions.
6. For the moment being, there is no clear abnormality in Au-Au collisions at 200 GeV. Further measurements to precisely quantify cold nuclear effects are a must.
7. J/ψ absorption, as observed in Pb-Pb collisions, affects only low p_T J/ψ 's for peripheral collisions. Higher p_T J/ψ 's are more and more suppressed with increasing centrality of the collision. This feature requires a robust experimental reference in order to allow model-independent conclusions.
8. The surviving J/ψ 's in Pb-Pb collisions exhibit an average $\langle p_T^2 \rangle$, or equivalently, a temperature T_{eff} which starts by increasing with increasing collision centrality. It saturates for energy densities above $\simeq 2.8 \text{ GeV}/\text{fm}^3$ and up to $3.9 \text{ GeV}/\text{fm}^3$, the average value of the most central bin.

Outlook

The theoretical analysis of the in-medium behaviour of quarkonia has greatly advanced in the past decade. Potential model studies based on lattice results for the colour-singlet free energy as well as direct lattice calculations appear to be converging, and within a few more years, the dissociation temperatures for the different quarkonium states will be calculated precisely. Through corresponding calculations of the QCD equation of state, these temperatures provide the energy density values at which the dissociation occurs. In statistical QCD, quarkonia thus allow a spectral analysis of the quark-gluon plasma.

The application of this analysis in high energy nuclear collisions is so far less conclusive. There exists a wealth of data from different interactions at the SPS, and first RHIC results are now also available. These results indicate the production of a hot, dense, strongly interacting medium. It is not yet clear, however, to what extent this medium is indeed the quark-gluon plasma studied in statistical QCD. Is it possible to identify dissociation onsets for different charmonium states? Does the initial (non-thermal) overabundance of charm survive a subsequent thermalization? Is the apparent J/ψ suppression saturation from SPS up to fairly central RHIC collisions the survival of the directly produced J/ψ 's as seen in lattice QCD studies, or is it the production of additional J/ψ 's through secondary $c\bar{c}$ pairings? These questions can only be answered by further experiments, ideally in all the possible energy ranges.

Future nucleus-nucleus experiments at the CERN-LHC will extend the field to much higher energy densities; but the precise experimental measurement of cold matter nuclear effects in this new energy domain will still remain the prime condition for the understanding and interpretation of the results.

References

- [1] T. Matsui and H. Satz, *Phys. Lett. B* 178 (1986) 416.
- [2] J. J. Aubert et al., *Phys. Rev. Lett.* 33 (1974) 1404;
J. E. Augustin et al., *Phys. Rev. Lett.* 33 (1974) 1406.
- [3] S. W. Herb et al., *Phys. Rev. Lett.* 39 (1977) 252.
- [4] F. Karsch, M.-T. Mehr and H. Satz, *Z. Phys. C* 37 (1988) 617.
- [5] F. Karsch and H. Satz, *Z. Phys. C* 51 (1991) 209
- [6] F. Karsch, M.-T. Mehr and H. Satz, *Z. Phys. C* 37 (1988) 617.
- [7] S. Jacobs, M. G. Olsson and C. Suchyta, *Phys. Rev.* 33 (1986) 3338.
- [8] E. Eichten et al., *Phys. Rev. D* 17 (1978) 3090; *Phys. Rev. D* 21 (1980) 203.
- [9] H. Satz, *J. Phys. G* 32 (2006) R25.
- [10] D. Kharzeev and H. Satz, *Phys. Lett. B* 334 (1994) 155
- [11] M. E. Peskin, *Nucl. Phys. B* 156 (1979) 365;
G. Bhanot and M. E. Peskin, *Nucl. Phys. B* 156 (1979) 391.
- [12] S. Matinyan and B. Müller, *Phys. Rev. C* 58 (1998) 2994.
- [13] L. Maiani et al., *Nucl. Phys. A* 741 (2004) 273.
- [14] D. Kharzeev and H. Satz, *Phys. Lett. B* 356 (1995) 365.
- [15] H. Miyazawa, *Phys. Rev. D* 20 (1979) 2953;
V. Goloviznin and H. Satz, *Yad. Fiz.* 60N3 (1997) 523
- [16] O. Kaczmarek et al., *Prog. Theor. Phys. Suppl.* 153 (2004) 287;
O. Kaczmarek and F. Zantow, *Phys. Rev. D* 71 (2005) 114510.
- [17] P. Petreczky and K. Petrov, *Phys. Rev. D* 70 (2004) 054503.
- [18] F. Karsch, E. Laermann and A. Peikert, *Phys. Lett. B* 478 (2000) 447.
- [19] F. Karsch, *Lect. Notes Phys.* 583 (2002) 209.
- [20] A. Peikert, F. Karsch and E. Laermann, *Nucl. Phys. B* 83-84 (2000) 390.

- [21] V. V. Dixit, *Mod. Phys. Lett. A* 5 (1990) 227.
- [22] S. Digal, P. Petreczky and H. Satz, *Phys. Lett. B* 514 (2001) 57.
- [23] S. Digal et al., *Eur. Phys. J. C* 43 (2005) 71.
- [24] O. Kaczmarek and F. Zantow, *Eur. Phys. J. C* 43 (2005) 63.
- [25] H. Satz, invited talk at SQM08, Beijing
- [26] E. Shuryak and I. Zahed, *Phys. Rev. D* **70**, 054507 (2004).
- [27] C.-Y. Wong, *Phys. Rev. C* 72 (2004) 034906;
C.-Y. Wong, hep-ph/0509088;
C.-Y. Wong, *Phys. Rev. C* 76 (2007) 014902.
- [28] W. Alberico et al., *Phys. Rev. D* 72 (2005) 114011.
- [29] D. Kharzeev, L. D. McLerran and H. Satz, *Phys. Lett. B* 356 (1995) 349.
- [30] S. Digal, P. Petreczky and H. Satz, *Phys. Rev. D* 64 (2001) 094015.
- [31] T. Umeda et al., *Int. J. Mod. Phys. A*16 (2001) 2215.
- [32] M. Asakawa and T. Hatsuda, *Phys. Rev. Lett.* 92 (2004).
- [33] S. Datta et al., *Phys. Rev. D* 69 (2004) 094507
- [34] H. Iida et al., *PoS LAT2005* (2006) 184.
- [35] A. Jacovac et al., *Phys. Rev. D* 75 (2007) 014506.
- [36] R. Morrin et al., *PoS LAT2005* (2006) 176;
G. Aarts et al., *Nucl. Phys. A* 785 (2007) 198.
- [37] Y. Nakahara, M. Asakawa and T. Hatsuda, *Phys. Rev. D* 60 (1999) 091503.
- [38] A. Mocsy and P. Petreczky, *Eur. Phys. J. C* 43 (2005) 77;
A. Mocsy and P. Petreczky, *Phys. Rev. D* 77 (2008) 014501.
- [39] W. M. Alberico et al., *Phys. Rev. D* 75 (2007) 074009;
W. M. Alberico et al., *Phys. Rev. D* 77 (2008) 017502.
- [40] C.Y. Wong and H. W. Crater, *Phys. Rev. D*75 (2007) 034505;
- [41] See e.g., N. Brambilla et al., *Heavy Quarkonium Physics*, CERN Yellow Report CERN-2005-005,
N. Brambilla et al., *Phys. Rev. D* 78 (2008) 014017.
- [42] N. Brambilla et al., *Phys. Rev. D* 78 (2008) 014017.
- [43] M. Laine et al., *JHEP* 0703 (2007) 054;
Y. Burnier, M. Laine and M. Vepsalainen, *JHEP* 0801 (2008) 043.

- [44] O. Philipsen, arXiv:0810.4685.
- [45] A. Beraudo, J.-P. Blaizot and C. Ratti, Nucl. Phys. A 806 (2008) 312; arXiv:0812.1130.
- [46] M. B. Einhorn and S. D. Ellis, Phys. Rev. D12 (1975) 2007;
H. Fritzsche, Phys. Lett. 67B (1977) 217;
M. Glück, J. F. Owens and E. Reya, Phys. Rev. D17 (1978) 2324;
J. Babcock, D. Sivers and S. Wolfram, Phys. Rev. D18 (1978) 162.
- [47] See, e.g., A. D. Martin, R. G. Roberts and W. J. Stirling, Int. Journal of Mod. Phys. A 10 (1995) 2885.
- [48] H. Satz and X.-N. Wang (Eds.), *Hard Processes in Hadronic Interactions*, Int. J. Mod. Phys. A 10 (1995) 2881;
M. Mangano et al. (Eds.), *Hard Probes in Heavy-Ion Collisions at the LHC*, CERN Yellow Report 2004-09, Geneva 2004.
- [49] R. Hagedorn, Nuovo Cim. Suppl. 3 (1965) 147;
Nuovo Cim. 56A (1968) 1027.
- [50] F. Becattini, Z. Phys. C 69 (1996) 485;
F. Becattini and U. Heinz, Z. Phys. C 76 (1997) 269.
- [51] J. Letessier, J. Rafelski and A. Tounsi, Phys. Rev. C64 (1994) 406.
- [52] P. Castorina, D. Kharzeev and H. Satz, Eur. Phys. J. 52 (2007) 187;
F. Becattini et al., Eur. Phys. J. C 56 (2008) 493.
- [53] P. L. McGaughey et al., Int. J. Mod. Phys. A 10 (1995) 2999.
- [54] R. Baier and R. Rückl, Z. Phys. C 19 (1983) 251.
- [55] G. T. Bodwin, E. Braaten and G. P. Lepage, Phys. Rev. D 51 (1995) 1125;
E. Braaten and S. Fleming, Phys. Rev. Lett. 74 (1995) 3327.
- [56] T. Affolder et al. (CDF), hep-ex/0004027;
E. Braaten et al., hep-ph/9911436.
- [57] See, however, H. Haberzettl and J.-P. Lansberg, Phys. Rev. Lett. 100 (2008) 032006.
- [58] D. Kharzeev and H. Satz, Phys. Lett. B 366 (1996) 316.
- [59] Y. Lemoigne et al., Phys. Lett. 113B (1982) 509;
L. Antoniazzi et al., Phys. Rev. D 46 (1992) 4828; Phys. Rev. Lett. 70 (1993) 383;
HERA B.
- [60] F. Abe et al. (CDF), Phys. Rev. Lett. 75 (1995) 4358;
T. Affolder et al. (CDF), Phys. Rev. Lett. 84 (2000) 2094.

- [61] D. Kharzeev and K. Tuchin, Nucl. Phys. A 770 (2006) 40.
- [62] M. J. Leitch, Eur. Phys. J. C 43 (2005) 157.
- [63] R. Vogt, Phys. Rev. C 61 (2000) 035203.
- [64] See e.g., K. J. Eskola, H. Paukkunen and C. A. Salgado, JHEP (2008) 0807:102, and references to earlier work given there.
- [65] D. Kharzeev and H. Satz, Z. Phys. C60 (1993) 389.
- [66] D. Kharzeev et al., Z. Phys. C74 (1997) 307.
- [67] D. Kharzeev, E. Levin and M. Nardi, Nucl. Phys. A 730 (2004) 448.
- [68] R. Vogt, Phys. Rev. C71 (2005) 054902.
- [69] D. Kharzeev and M. Nardi, Phys. Lett. B 507 (2001) 121.
- [70] S. J. Brodsky and A. H. Mueller, Phys. Lett. 206 B (1988) 685;
N. Armesto and A. Capella, Phys. Lett. B 430 (1998) 23.
- [71] D. Kharzeev, F. Karsch and H. Satz, Phys. Lett. B 637 (2006) 75.
- [72] P. Braun-Munzinger and J. Stachel, Nucl. Phys. A690 (2001) 119.
- [73] R. L. Thews et al., Phys. Rev. C 63 (2001) 054905.
- [74] L. Grandchamp and R. Rapp, Nucl. Phys. A 709 (2002) 415.
- [75] P. Braun-Munzinger and J. Stachel, arXiv:0901.2500.
- [76] For a recent work, see C. Pajares, Eur. Phys. J. C 43 (2005) 9;
D. Kharzeev et al., arXiv:0809.2933.
- [77] F. Becattini et al., hep-ph/0508188
- [78] S. Gupta and H. Satz, Phys. Lett. B 283 (1992) 439.
- [79] For a recent survey, see R. L. Thews, Eur. Phys. J. C 43 (2005) 97.
- [80] R. L. Thews and M. Mangano, Phys. Rev. C 73 (2006) 014904;
R. L. Thews, hep-ph/0510390.
- [81] D. Kharzeev, M. Nardi and H. Satz, Phys. Lett. B 405 (1997) 14.
- [82] S. Gavin and M. Gyulassy, Phys. Lett. B 214 (1988) 241;
J. Hüfner, Y. Kurihara and H. J. Pirner, Phys. Lett. B 215 (1988) 218;
S. Gupta and H. Satz, Phys. Lett. B 283 (1992) 439.
- [83] F. Karsch and R. Petronzio, Phys. Lett. B 212 (1988) 255.
- [84] J. P. Blaizot and J.-Y. Ollitrault, Phys. Lett. B 217 (1988) 392.

- [85] H. Liu, K. Rajagopal and U. A. Wiedemann, Phys. Rev. Lett. 97 (2006) 182301.
- [86] O. Kaczmarek et al., Phys. Lett. B 543 (2002) 41; Phys. Rev. D 70 (2004) 074505.
- [87] H. Satz, arXiv:0812.3829 [hep-ph].
- [88] M.C. Abreu *et al.*, (NA50 Coll.), Phys. Lett. B 410 (1997) 327.
- [89] C. Gerschel and J. Huefner, Phys. Lett. B 207 (1988) 253. C. Gerschel and J. Huefner, Z. Phys. C 56 (1992) 171.
- [90] M.C. Abreu *et al.*, (NA51 Coll.), Phys. Lett. B 438 (1998) 35.
- [91] M.C. Abreu *et al.*, (NA38 Coll.), Phys. Lett. B 444 (1998) 516.
- [92] C. Lourenço, Nucl. Phys. A 610 (1996) 552c.
- [93] N. S. Topilskaya et al. (NA50 Coll.), Nucl. Phys. A 715 (2003) 675.
- [94] B. Alessandro *et al.*, (NA50 Coll.), Phys. Lett. B 553 (2003) 167.
- [95] M.C. Abreu *et al.*, (NA50 Coll.), Phys. Lett. B 410 (1997) 337.
- [96] B. Alessandro et al. (NA50 Coll.), Eur. Phys. J. C 48 (2006) 329.
- [97] G. Borges, PhD Thesis, Universidade Técnica de Lisboa-IST, Lisbon, 2005.
- [98] B. Alessandro et al. (NA50 Coll.), Eur. Phys. J. C 39 (2005) 335.
- [99] M.C. Abreu *et al.*, (NA38 Coll.), Phys. Lett. B 466 (1999) 408.
- [100] J. Badier et al., (NA3 Coll.), Z. Phys. C 20 (1983) 101.
- [101] L.Kluberg (from G. Borges), slides presented at HP2004, Ericeira, Portugal. Unpublished.
L. Kluberg, Eur. Phys. J. C 43 (2005) 145.
- [102] G.A. Schuler, Habilitationsschrift, Univ. Hamburg, Germany, 1994, CERN-TH-7170-94, arXiv:hep-ph/9403387.
- [103] M.C. Abreu et al., (NA50 Coll.), Phys. Lett. B 530 (2002) 43.
- [104] B. Alessandro et al., (NA50 Coll.), Physics Letters B 499 (2001) 85.
- [105] N. S. Topilskaya et al.(NA50 Coll.), in *Relativistic Nuclear Physics and Quantum Chromodynamics*, A. N. Sissakian, V. V. Burov and A. I. Malakhov (Eds.), Dubna JINR 2005, p. 255 - 262.
B. Alessandro et al., (NA50 Coll.), Nucl.Phys. A 749 (2005) 243.
- [106] C. Baglin et al., (NA38 Coll.), Phys. Lett. B 262 (1991) 362.
- [107] M.C. Abreu et al., (NA38 Coll.), Phys. Lett. B 423 (1998) 207.

- [108] R. Hagedorn, Riv. Nuovo Cimento 6 (1938) 1.
- [109] J.D. Bjorken, Phys. Rev. D 27 (1983) 140.
- [110] B. Alessandro et al., (NA50 Coll.), Eur. Phys. J. C33 (2004) 31.
- [111] R. Shahoyan, PhD Thesis, Universidade Técnica de Lisboa-IST, Lisbon, 2001.
- [112] B. Alessandro et al., (NA50 Coll.), Eur. Phys. J. C 49 (2007) 559.
- [113] H. Santos, PhD Thesis, Universidade Técnica de Lisboa-IST, Lisbon, 2004.
- [114] R. Arnaldi et al., (NA60 Coll.), Phys. Rev. Lett. 99 (2007) 132302.
- [115] S. S. Adler et al., (PHENIX Coll.), Phys. Rev. Lett. 92 (2004) 051802.
- [116] A. Adare et al., (PHENIX Coll.), Phys. Rev. Lett. 98 (2007) 232002.
- [117] S. S. Adler et al., (PHENIX Coll.), Phys. Rev. Lett. 96 (2006) 012304.
- [118] A. Adare et al., (PHENIX Coll.), Phys. Rev. C 77 (2008) 024912.
- [119] A. Adare et al., (PHENIX Coll.), Phys. Rev. Lett. 101 (2008) 122301.
- [120] S. S. Adler et al., (PHENIX Coll.), Phys. Rev. C 69 014901 (2004).
- [121] A. Adare et al., (PHENIX Coll.), Phys. Rev. Lett. 98 (2007) 232301.
- [122] K. Adcox et al., (PHENIX Coll.), Nucl. Instrum. Methods Phys. Res., Sect. A 499 (2003) 469.
- [123] R. Granier de Cassagnac, J. Phys. G35 (2008) 104023.
- [124] M.J. Leitch et al., (E866/NuSea Coll.), Phys. Rev. Lett. 84 (2000) 3256.
- [125] P. Charpentier, Thèse, Université de Paris Sud, Orsay, 1983.
- [126] A. Adare et al., (PHENIX Coll.), Phys. Rev. C 77 024912 (2008) 024912.